An Ecological and Engineering Approach to Optimizing Algal Biofuels

by

David Neil Carruthers

A thesis submitted
in partial fulfillment of the requirements
for the degrees of
Master of Science
(Chemical Engineering)
Master of Science
(Natural Resources and Environment)
at the University of Michigan
April 2016

Faculty advisors:

Dr. Xiaoxia (Nina) Lin, Associate Professor, Chemical Engineering Department
Dr. Bradley Cardinale, Professor, School of Natural Resources & Environment

Abstract:

Algae are ubiquitous in natural ecosystems and have been studied extensively due to their versatility for biofuel production. Most of these studies have been conducted on the grounds of synthetic biology and process engineering with few industrial scale projects considering algal community interactions. Such interactions have often indicated the propensity of increasing overall productivity and reducing community invasability, both important characteristics for scalable projects. However, over 30,000 species of algae have currently been identified with another 20,000 estimated to exist. Within this context, elucidation of these relationships remains extremely resource and time intensive.

This thesis outlines a strategy for rapid, high-throughput screening of algal community combinations using a microfluidic platform to synthesize millions of parallel, nanoliter-scale algal communities for analysis of biomass accumulation. Model communities were first studied in a bench scale flask experiment and then examined using microfluidic droplets. These experiments showed consistent results on both positively and negatively interacting algal bicultures. Specifically, these include better performance within bicultures of *Ankistrodesmus falcatus* and *Chlorella sorokiniana* as well as *Chlorella sorokiniana* and *Selenastrum minutum* with lower performance within the biculture of *Selenastrum capricornutum* and *Scenedesmus ecornis*.

Biofuels provide a unique opportunity for market penetration in one dominated by petroleum based fossil fuels. They serve as renewable and significantly less carbon intensive alternatives. While the holistic success of algal biofuels will hinge on an amalgamation of these scientific fields, rapid screening of algal communities could prove imperative for discovering community interactions and ideally facilitating a mechanistic analysis of how such interactions arise in natural communities.

Acknowledgements:

Firstly I'd like to thank my producer, microalgae, for facilitating this paper. It's really been a positive community effort.

But honestly, to my loving family; Mom, Dad, Andrew, and Kimberly, for their tireless love, motivation, and support. To my PI, Nina Lin for her continued support in my academic endeavors, Brad Cardinale for his collaboration and expertise, and the School of Natural Resources and Environment for an excellent experience.

Table of Contents

Chapter 1: Algal biofuel production

1.1 National energy security and climate change

The US Energy Information Administration (EIA) estimates that in 2015 the United States consumed 19.4 million barrels of petroleum per day for transportation, a figure accounting for the emissions of nearly 2.252 million tonnes of carbon dioxide[1]. Over the last decades, transportation emissions have drawn increased scrutiny due to their enormous proportion of total greenhouse gas emissions, the inherently unsustainable nature of fossil fuels, and forecasted increases in petroleum consumption on a global level. Even with estimates of 25 years of stable petroleum production on the basis of proven and unproven reserves, recent projects have ventured into riskier territories faced with increased public resistance[2]. Projects include the expansion of hydraulic fracturing techniques and drilling proposals for remote locations such as the Arctic National Wildlife Refuge or deep offshore waters[2]. The negative consequences of such projects are epitomized by the Exxon-Valdez and Deepwater Horizon catastrophes in the short term and global climate change in the long term, both of which pose tremendous threats to national energy security[3]. As of 2007, changing of the global climate has been deemed unequivocal within the scientific community with 97% of experts asserting such changes are at least partially anthropogenic[4].

Current approaches to global sustainability tend toward carbon emissions reduction typified by top-down legislative control instigated broadly by the United Nations Framework Convention on Climate Change (UNFCC) and public information supplied by the Intergovernmental Panel on Climate Change (IPCC) [5]. Such legislative mechanisms remain biased towards emission abatement via cap-and-trade programs and similar economic incentives, which tend to exacerbate imbalances between industrialized and developing nations. While undoubtedly successful in some instances, these mechanisms ultimately fail to address the magnitude of modern carbon emissions in their entirety. The UNFCC's Paris Conference of Parties (COP) in 2015 established an agreement characterized by a consolidated effort to keep global climate change below the threshold of $2.0^{o}C$ above pre-industrial levels. This seemingly arbitrary threshold is one widely accepted to be best achievable and best capable of mitigating sea level rise, weather variability, biodiversity losses, and declining crop yields among the many other dire consequences of climate change[6]. Achieving such a threshold will

necessitate leaving some fossil fuel reserves in the ground, a reality the world is simply not ready to embrace.

A number of important movements to address these emissions have begun to increase global sustainability and attain increasingly rigorous carbon dioxide emission reductions. These include the $100 billion dollars pledged by COP nations in 2015 as well as increased international investment in green bonds, funds dedicated towards sustainable project development[7]. Even so, such funding cannot singly attain the prescribed goals of the COP nor avoid the projected consequences of global climate change. It will demand a multifaceted approach that includes behavioral and sociopolitical balance alongside scientific advances in efficiency and fuel development. One opportunity in fuel development pertains to robust scientific advances in metabolic and ecosystem engineering that facilitate bottom-up control with the development of genetically modified communities. Recent petroleum volatility and the explosion of biotechnological companies have stimulated increased research in the development of biofuels with an enormous potential for market penetration.

1.2 Viable biofuel development and production strategies

Biofuels have gained particular attention in the last decade due to an upswing in national and energy security. Their development has been facilitated largely by US EPA's Renewable Portfolio Standards, established as an integral component of the Energy Act of 2005 [8]. Based on choice process pathway, fuel products range from ethanol, bio-crude, biodiesel, methane, to hydrogen. Relevant substrates include canola, corn, palm, soybean, algae, tallow, and lignocellulosic biomass with most of which optimized a specified fuel pathway[9]. In the United States, biofuel production is dominated by corn ethanol, which accounted for 94% of all biofuel production in 2012 [10]. Under the most ideal circumstances, extrapolation of current biofuel production capacity would require the majority of the land area of the United States given current market demands. This level of production is fundamentally impractical.

The dominant narrative in biofuel synthesis involves the development of genetically modified organisms (GMOs). This framework has not only demonstrated the capabilities of metabolic engineering through enhanced lipid production, but its broad ability to manipulate a seemingly innocuous target strain into a product with industrial viability and the potential to meet market demands. Nonetheless this approach is hampered by the consequences of

horizontal gene transfer, genetic functional trade-offs in metabolism, and the inherent instability of monocultural farming with respect to resilience to disturbances and predators.

The substantial research and development allotted to biofuel synthesis have led to the derivation of five fundamental characteristics of biofuel viability:

1. Economic parity with petroleum by levelized cost of energy calculations.
2. An energy return on energy investment above 1.0, as calculated following the International Organization for Standardization 14040 principles and the framework for life cycle assessment. Together, these define potential impacts associated with biofuel products throughout their life cycle[11].
3. Minimal land use change of the natural environment or current arable land for food resources, the implications of such land loss involve habitat loss, carbon sequestration loss, urban heat sinks, etc[12].
4. Minimal water intensity, fertilizer requirements, and lifecycle carbon footprint through the incorporation of aqueous or nutrient recycling methods.
5. Sustained, reliable energy generation that continually meets market demand while ultimately reducing tailpipe emissions.

Following these criteria, the ideal biofuel would be one readily synthesized by a fast growing, dense source of biomass compatible with the current fuel infrastructure with negligible life cycle carbon emissions, such that it is salable, sustainable, and scalable. While these collective characteristics are not present in any known organism, certain organisms have advantageous traits. Microalgae and microbes capable of digesting lignocellulosic biomass show promise in their viability for the production of cleaner, renewable sources of energy with respect to their fossil fuel analogues. Furthermore, they provide an attractive opportunity for industrial development due to their inherent compatibility with the current petroleum-based infrastructure. Replacing fossil fuels with a cost effective, renewable alternative in a competitive energy market could ubiquitously reduce carbon emissions. However, the methods with which algae may be engineered competitively in such a market remain especially challenging.

1.3 Microalgae as a source for biofuel production

Microalgae maintain an enormous level of diversity. There are currently a projected total of 50,000 species of microalgae, of which 30,000 have been studied and characterized on the basis of productivity, byproduct synthesis, and environmental constraints[13]. They remain an especially promising biofuel source foremost due to their relatively low space requirements and their noncompetitive nature with human food resources. Likewise, their particularly high photon conversion rate allows for high growth rates, despite diurnal and annual temperature and light fluctuations, and sustainable cultivation in massive outdoor ponds[14]. It is estimated that algae have the potential of producing up to 50,000 kg/acre/year of biomass, an appealing trait in the context of biofuel production[14]. These species include some of the simplest photoautotrophic organisms, which use photosynthetic machinery to convert sunlight to chemical energy, enabling the synthesis of organic compounds for cell function. In recent years, these characteristics and algae associated economic viability have contributed to the establishment of a highly developed molecular toolkit that includes chloroplast gene targeting and genomic sequencing, as typified with the model organism *Clamydomonas reinhardtii*[15]. Varying processing techniques have demonstrated production of biodiesel, bioethanol, biogas, biohydrogen, and biocrude, which correspond to lipids, sugars/starches, sulfur deprivation in an anaerobic environment, and overall biomass. In juxtaposition, current popular biofuel sources like corn, canola, and sugar cane are limited to one or two fuel pathways[16].

The largest disparity between laboratory cultivation and pond or raceway macrocultivation is the variability of conditions, including light and temperature, fitness against invasion, longevity of genetic stability, and nutrient demands[17]. Engineering specific strains for production capacity, while useful, cannot be considered as the standalone approach to algal biofuel research. A framework for algal biofuel research has been proposed discussing an optimization of biological, ecological, and reactor engineering to maximize production.

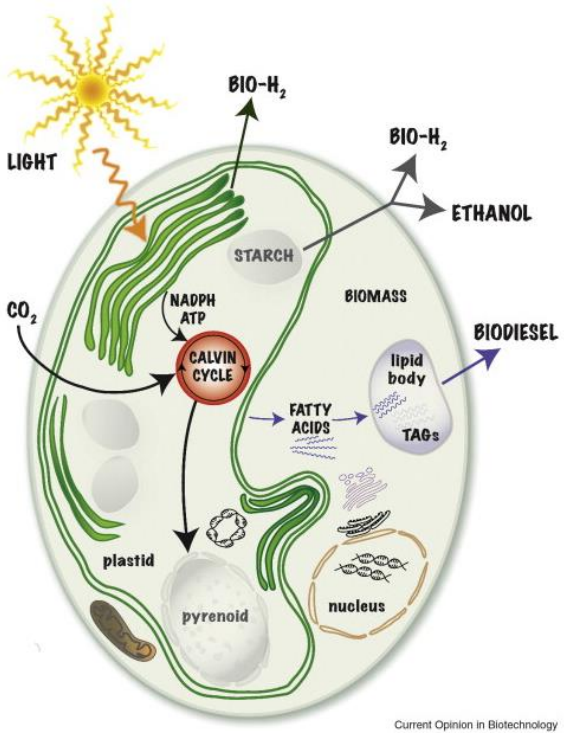

Figure 1: Generic illustration of algal biofuel production from specified metabolic machinery in microalgae. Adapted from Beer et al. (2009).

1.3.1 Synthetic biology and metabolic engineering

The sheer diversity of microalgae provides a plethora of possible targets for biofuel production though most current efforts in genetic engineering gravitate to tailoring an idealized algae super strain. Synthetic biology in microalgae leans towards the manipulation of specific metabolic pathways through a varied approach using the well-defined tools of molecular biology. Routine genetic manipulation is largely limited to several species of model microalga: *Clamydomonas reinhardtii, Volvox carteri, and Phaeodactylum tricornutum*[18]. Approaches include expression of transgenes, gene regulation, inducible nuclear promoters, and inducible chloroplast gene expression by means of some combination of mutagenesis, reverse genetics, and homologous recombination of gene transformants[18]. Photosynthetic efficiency has also been intensely explored with the study of light-harvesting antennae complexes (LHC) composed of arrays of chlorophyll and protein molecules located in chloroplast thylakoid membrane in chloroplast photosystems. These studies provided recognition of important genes for chloroplast regulation[19]. Modification of LHC size has mitigated the effects of cellular shading, improving population efficiency[21].

Another approach is geared towards manipulating the Calvin cycle, which uses ATP and NADPH to convert fixed carbon dioxide and water into useful organic metabolites. The

fixation process converts CO_2 into ribulose-1,5-biphosphate[20]. This biochemical is then catalyzed by the enzyme RuBP carboxylase/oxygenase (nicknamed RuBisCo) to form 3-phosphoglycerate, the fundamental product of the cycle[20]. This process utilizes an enormous proportion of cellular energy and, while fundamental to photosynthesis, RuBisCo is a particularly inefficient enzyme that creates a metabolic bottleneck in carbon flux within the cell[22]. Optimization of this process could facilitate increased carbon fixation thereby, if limiting, facilitating increased biomass accumulation within the population. The principles of both photosystem and RuBisCo engineering aim to increase cellular efficiency thereby allowing for production of pertinent coproducts[22].

Lastly, a fundamental strategy for algal optimization involves gene replacement by homologous recombination. This follows a specified framework of gene isolation, amplification, ligation, transformation by particle bombardment, and screening for homoplasmic colonies under a selective pressure. This strategy has demonstrated production of novel synthetic proteins, including vaccines, immunotoxins, and pharmaceutical products[16]. While not necessarily pertinent to biofuel production, this strategy may also be used to modify genes or gene promoters in order to amplify targeted gene expression in specified metabolic pathways as indicated by specific reporters.

While these strategies have each demonstrated the power of synthetic biology in the restructuring of cellular machinery, inherent functional trade-offs and the complexity of relevant algae strains set limits on application. For example, while *C. reinhardtii* is particularly well studied, techniques may not be directly translatable to other algal strains due to evolutionary differences. Furthermore, aquatic ecological studies have indicated that monocultures tend to have less temporal stability than species, particularly in terms of invisibility and productivity.

1.3.2 Process engineering

Each methodology of algal biofuel processing begins with a raw algal biomass slurry, though specified catalysts and reactants affiliated with the desired pathway. Algal biomass may be grown in an open pond raceway or photobioreactor depending on regional specifications consisting of sunlight availability, evaporation, diurnal cycling, and so forth. The principle strategies of fuel production summarized below are largely translatable from the cell

description of Figure 1.

Table 1: Algal biofuels by process and relevant metabolic pathway

Process	Products	Pathway	Reference
Anaerobic Digestion	Methane, carbon dioxide	Spent biomass	Radakovits et al. (2010)
Transesterification	Biodiesel, glycerol	Fatty acid biosynthesis	Radakovits et al. (2010)
Hydrothermal Liquefaction	Bio-crude	Whole biomass	Chiaramonti et al. (2016)
Pyrolysis	Bio-crude, syngas	Whole biomass	Chiaramonti et al. (2016)
Gasification	Syngas, methane	Process wastewater, spent biomass	Stucki et al. (2009)
Hydrogenesis	Hydrogen	Photosynthesis in anaerobic conditions	Ghiardi et al. (2000)
Fermentation	Ethanol	Starch synthesis, cellulose	Harun et al (2011)

A majority of process research in algal biofuels has been dedicated to the optimization of transesterification, the process by which triacylglycerides are reacted with methanol in the presence of a homogenous alkali base catalyst, generating glycerol and fatty-acid methyl esters. On the other hand, the majority of general biofuel production has focused on the fermentation of corn mash for the production of ethanol. Each process listed above has distinctive differences from its partners. Gasification and anaerobic digestion are both methods by which algal wastewater or spent biomass may be recycled for generation of gaseous fuels though these processes are generally used in tandem with pyrolysis, hydrothermal liquefaction (HTL), fermentation, or transesterification to reduce overall waste and increase EROI.

The dominant considerations in selecting an algal pathway are dewatering, which is particularly energy intensive given the dilute nature of algal cultures, and nutrient management[24]. HTL is an emergent technology that uses elevated temperatures and pressures to synthesize biocrude from whole algal biomass within a relatively short reaction time[24]. Experimental yields have indicated a maximum generation of 64 wt % biocrude with biocrude

and gas products capturing an estimated 90% of total energy from the algal feedstock[24]. This appears immediately promising due to the lack of dewatering as well as recent breakthroughs indicating the viability of bacterial and algal cultivation on HTL aqueous process waste. These strategies provide increased nutrient retention and increased overall biomass generation[24,25]. The tunability of experimental temperature, pressure, and reaction time facilitate application to other algal species and, more importantly, specified nutrient outputs of phosphorous, nitrogen, oxygen and slurry co-products for determination of ideal production conditions. The benefits of HTL also mean that the accumulation of biomass becomes increasingly important. Engineering communities of facilitative algal species could thus reduce incubation time and increase fuel yields.

1.3.3 Ecological engineering and species selection

Ecological engineering involves the selection of strains that demonstrate a predisposition for increasing targeted productivity within a given community. Such productivity is intimately connected with intracellular and intercellular interactions, which may pertain to metabolite exchange or, more broadly, to niche partitioning. While this approach is markedly different from that of synthetic biology, which attempts to manipulate the metabolic machinery of a single species for optimal production of a target, it involves the manipulation of intercellular phenomena and characteristics seemingly inherent to biodiverse communities. A strategy that could be particularly useful for algal biofuel production incorporates tailoring a community for the creation of a specific product by translating laboratory experiments to outdoor raceways or ponds.

Biodiversity may be classified as the differences in composition between two regions through measures of total species richness and the proportion of said communities[26]. The ecological definition of a community is an unspecified group of species that occur together in any arbitrary space and time, often varying in specificity between different trophic levels[26]. Diversity, in this context, is particularly useful due to the apparent collective community resistance to invasion, external natural perturbations, and profound effects on ecosystem functioning[26]. These relationships have been demonstrated within grassland communities as explored by the seminal research of Tillman et al. in 1994 [27]. An analysis of biomass accumulation in grassland plots over a two-year drought period indicated those with a higher

species richness had a significantly greater impact on overall plot drought resistance, classified by a log ratio of pre-drought and post-drought biomass per plot[27]. Subsequent studies in unstressed grassland communities indicated that primary production increased linearly with species richness[28,29]. Extrapolation to experiments with multiple trophic levels also indicated that the most diverse communities tended to have a positive impact on increased CO_2 production and overall productivity, again defined as biomass generation[30]. These experiments, among others, were designed to test the diversity-stability hypothesis. The hypothesis states that interacting species tend to dampen potentially destabilizing interactions either between consumer-resource or predator-prey relationships[31]. Interactions are further complicated by the trophic complexity of the ecosystem and equilibria between species. These are best described by the niche complementarity hypothesis, which states that ecosystem functioning is directly related to species resource use[26]. If use between species varies significantly, the overall resource use and thereby community production will increase[26]. This hypothesis is particularly relevant for a community in which multiple producers coexist and is juxtaposed against the competitive exclusion principle, by which two species cannot coexist on a single limiting resource. This ultimately leads to the characterization of ecological niches by which specific species within a community are best suited[32]. Such niches are characterized by both abiotic and biotic dimensions between interspecies interactions and overall resource availability. If niche complementarity or niche partitioning is sufficiently strong, then the net increase in biomass may be substantially measured, lending to the term transgressive overyielding. This is a simple comparison of the community biomass production with respect to that of the individual species[33]. The degree to which this phenomenon takes place is largely dependent on the nature of community, specifically the relative carrying capacities and growth rates of subspecies[26]. Regardless, this has been clearly demonstrated in terrestrial systems as discussed in Tillman et al., and, more recently, in aquatic communities.

While tending to overlook the mechanisms with which these interactions occur (metabolite exchange, niche partitioning, microbial symbionts, etc), these results are promising in their relation to the seemingly troubling characteristics of large scale algal production. Algal ponds facilitate a single species in its fundamental niche, relatively independent of interspecific interactions. Under these circumstances, the role of niche differences between interacting species regulate nutrient uptake becomes increasingly relevant. Microbial partnerships of this

nature have been explored with an example being the unexpected symbiosis between *Porphyridium purpureum*, a marine red alga, and *Halomonas sp.,* a bacterial species marked for increased cobalamin (Vitamin B_{12})[34]. These experiments demonstrated the symbiosis within an algae-bacteria coculture with resultantly increased biomass with the important determination of the limiting resource, i.e. the lack of vitamin B_{12} biosynthesis in *P. purpureum*[34]. The potential for algal regrowth on waste media is also particularly appealing from the perspective of a consolidated recycling stream. This stream has been studied variably with the regrowth of bacterial, algal, and yeast monocultures on HTL waste dilutions with generally positive results[24,25]. This indicates the plausibility of manipulating microbial community interactions for the purpose of targeted product development.

Laboratory algal polycultures have demonstrated niche partitioning as indicated specifically in a study of freshwater stream water quality[35]. Cardinale et al. 2007 indicate that algal polycultures produce an average of 1.7 times more biomass than individual monocultures, with increased productivity in 79% of all experiments[36]. However, in terms of transgressive overyielding, only 12% of polycultures demonstrated higher biomass than their constitutive most productive monoculture[36]. The average polyculture ratio with respective to the constitutive highest producing monoculture was 0.87 [36]. Cardinale et al. 2011 also indicate that, in a selection of almost 60 terrestrial and aquatic systems, polycultures reported on average 48% less final nutrients than constituent monocultures though, again, not as efficiently as the most efficient monocultures[37]. Nonetheless, these results are promising not only in elucidating particularly useful algal strains, but in providing that there are in fact certain combinations of algal interactions that tend to increase overall productivity in specific combinations. These relationships are likely classified as mutualism or facilitation, which indicate an enhancement of growth, survival, or reproduction in another species[26]. Symbioses, as typified by the marriage between *P. purpureum* and *Halomonas sp.* are different in that they represent present and intimate positive relationships in stable coexistence[34].

Prospecting for these overyielding relationships can be tedious, expensive, and extremely time consuming, especially given the aforementioned 30,000 identified species of algae. Likewise, these relationships become increasingly difficult to model to the limiting density dependence or limiting resource provisions of the individual species[26]. Some research has been conducted as a means to better understand the interrelatedness between overyielding

polycultures beyond niche differences, namely by considering evolutionary deviation through phylogenic distances. This is on the basis of the so-called competition-relatedness hypothesis, which proposes that species with low phylogenic distances tend to utilize similar resources or similar niches. Results of some studies indicated that increases in productivity were unrelated to phylogenic distances, while others indicated that phylogenetic closeness actually contributes to facilitation[38]. Rather, strain selection would highly benefit from the development of a high throughput platform by which algal polycultures could be quickly analyzed, relationships elucidated, and considered on the basis of productivity. Presumably these selected strains could then be considered as candidates for thermochemical processing, by which entire algal biomass could be converted to bio-crude product. This distinction is important as it serves as the simplest and cheapest mechanism by which viable algal biofuel could be manufactured. Therefore, strain selection could benefit substantially through the application of a microfluidic device and the slew of recent breakthroughs in photolithography, facilitating the development of total analytic systems with varied biological applications.

1.4 A holistic approach

The review above has discussed three integral strategies for economically viable algal biofuel production with a principle strategy being the inclusion of ecological factors. These factors have been largely overlooked in large scale pond processing beyond that of resistance to invasion and could facilitate the economic viability of algae, a prospect of increasing necessity in a fossil fuel driven world. Estimates indicate that algal biofuels could reduce the emission of CO_2 in the transportation sector by up to 30% [39]. The plethora of strategies for biofuel production and biomass generation will also demand the employment of life cycle analysis and techno economic analysis, where combinations of generation and development may be compared for optimal salability, sustainability, and scalability[40]. Attainment of these goals will facilitate the transition to a less carbon intensive future.

Chapter 2: A microfluidic platform for species selection

2.1 Introduction

Microfluidics remains a dominant narrative in the application and refinement of contemporary engineering solutions to more complex systems via manipulation of the well-studied principles of fluid mechanics. Such studies have allowed for numerical modeling, parametric analyses, and systemic performance assessments for practical purposes. Of specific relevance to the study of algal communities are microfluidic devices for droplet generation, which has been ameliorated and incorporated within a robust range of research topics. A general principle in droplet formation is the manipulation of two immiscible fluids, typically via polarity, which allow the isolation of specific solvents in droplet volumes. A common demonstration of this phenomenon arises frequently in organic chemistry laboratory experiments in which an emulsion may form between aqueous and nonaqueous, usually nonpolar phases. Though uncontrolled, this emulsion is a key principle in microfluidic droplet formation.

These droplets, referred to broadly as the dispersed phase, do not interact with the surrounding medium, called the continuous phase, such that chemical syntheses or high-throughput screenings may be effectively employed[41]. Most importantly, this allows for effective separation of organic materials, which are readily soluble in oil, and other biological agents that are soluble in water, offering potential in revolutionizing medicinal drug delivery approaches. Microfluidics also appeals to these systems on a significantly finer scale, generally categorized between 10^{-9} to 10^{-18} liters[42]. Development in this manner stems from a combination of other microanalytical methods, namely gas-phase chromatography, high pressure liquid chromatography, and capillary electrophoreses [42]. These processes qualitatively define the basics of droplet formation in their analogous pertinence to extremely high sensitivity while involving small sample sizes.

In a similar fashion, microfluidic systems as a technical platform offer a unique insight into a range of contemporary engineering fields with recent advancements pairing well with the current shift towards microscale[43]. Miniaturization in this context enables the benefits of micro/nanotechnology, which include the conservation of reagents and precious reactive material, experimental expenses, and an increased general efficiency[43]. These benefits are

primarily achieved by tunability and controllability each droplet, which act as tiny bioreactors and allow for parallel processing such that large datasets may be quickly and easily compiled[44]. Likewise, the compartmentalization of chemical or biological systems in this manner facilitates the development and application of lab-on-a-chip type technology with extremely high resolution[43].

A range of Microfluidic Droplet Generators (MFDGs) have been developed as mechanisms for producing monodisperse droplets. The generators are generally narrowed into three fundamental categories: co-flow devices, T-junctions, and flow-focusing devices. These may be further complicated by the addition of pumps, valves, and similar microanalytical tools developed by etching poly(dimethylsiloxane) (PDMS) or a similar polymer[42]. This polymer is ideal because it is transparent, unreactive, inexpensive, and readily manipulated by fabrication processes. It can be etched by a number of versatile strategies including deposition, electrodeposition, and soft lithography, processes only refined in the early 2000's due to a reduction in cost and production time of relevant laboratory equipment[45].

Of primary concern in regards to these mechanisms is a determination of the factors that control droplet diameter and monodispersity, namely phase viscosity and interfacial tension. The practical applications of microfluidic design in this manner pertain to a wide array of chemical, biochemical, medicinal, and ecological indices, many of which are tailored to one of the specific aforementioned design criteria. Each case will be discussed on the basis of the prevalent fluid mechanics in engineering modeling software.

2.2 Droplet formation strategies

The formation of microfluidic droplets requires several key factors, namely mechanisms for introducing the reagents, moving these reagents on a chip, and drawing analytical solutions[42]. The chip itself is usually etched or molded using an elastomer mixture, such as PDMS in order to create a network of microchannels. These microchannels and their flows may be characterized by the Reynold's number, which incorporates the density and viscosity of the targeted medium as well as the characteristic dimension as calculated in the standard way:

$$Re = \frac{\rho u l}{\mu} \tag{1}$$

As suggested by the above equation, low dimensions lead to flows dominated by viscosity such that Re << 1 and, subsequently, the flow is laminar with negligible inertial forces[46]. As a result of this laminar constraint, intramixing of droplets is largely accomplished by means of internal diffusion rather than by turbulent flow[43]. This is an important distinction for modeling and understanding of biological nutrient uptake such that, for example, flasks on platform shakers are likely subject to a more homogeneous environment. The effects of homogeneity on algal culture growth and the relative effects of diffusion within microdroplets were not explored in this research.

The effectiveness of a droplet forming device pertains to its polydispersity index (PDI), a measure of the overall variation in droplet diameter. Consistent diameter remains of special importance for comparison of experimental reproducibility remains essential in device development and implementation. In this context PDI may be calculated as follows:

$$PDI = \frac{\sigma}{\mu} \tag{2}$$

Here, σ represents the standard deviation of droplet diameters and μ the mean diameter. This analysis can typically be conducted through high-speed cameras and imaging software[49].

A final characteristic of all droplet generators is the necessity to keep droplets under controlled coalescence to avoid improper fusion, which could skew experimental results[44]. This is of particular relevance to applications that study chemical kinetics or chemical synthesis, which require fusion at a specified time and rate. Manipulation in this manner can be accomplished by either passive or active fusion. In the former process, channel flow is manipulated so as to control droplet formation frequency, a characteristic controlled by channel geometry and overall flow rate[44]. These parameters allow for mixing at a set rate in the continuous channel. In an example of active fusion, electrodes are placed parallel to droplet channels with applied voltages allowing for significant control over droplet fusion[44]. Alternatively, the addition of electrodes allows control over particles through implementation of the electrowetting-on-dielectric (EWOD) type mechanism. Controlled coalescence is of critical concern for microbial communities, which must maintain their individual integrity over an extended period of time. In this case, surfactants may simply be mixed with the oil phase.

2.2.1 T-Junction devices

The T-junction method of monodisperse droplet formation remains one of the most frequently used microfluidic geometries namely due to the straightforwardness of its construction[46]. The first microfluidic chip of this nature was developed by Thorsen et al[47]. Droplets are formed by a dual injection of an aqueous phase, usually water, perpendicular to a non-aqueous phase, usually oil or another hydrophobic liquid that facilitates emulsion and, subsequently, droplet formation as the dispersed phase[43]. Experimentally, a scaling law has been drawn to indicate the reliance of droplet volume on the diameter of the channel:

$$\frac{V}{D^3} = 1 + \alpha * \frac{Q_{in}}{Q_{out}} \tag{3}$$

Here, V is the droplet volume, D is the diameter of the channel, and the constant α is to the order of unity, varying based on the MFDG. Excluding the coefficient α, this linear relationship is effectively independent of fluid properties[46]. Injection of the aqueous phase is often perpendicular or angled with respect to the flow of the latter phase such that shearing stresses dominate. Following Equation 3, droplet size increases with increasing dispersed phase pressure[48]. Likewise, Nsisako et al. (2002) reported a decreased droplet size with respect to decreased continuous phase velocity[49].

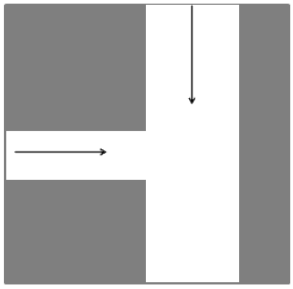

Figure 2: A depiction of a basic T-Junction with obvious attention drawn to the perpendicular entry of the dispersed phase. Likewise, the diameter of the vertical continuous phase channel appears significantly larger than that of the horizontal dispersed phase channel so as to facilitate shearing stresses and, subsequently, droplet formation.

Even in this simple model, manipulation of droplet diameter may be accomplished by changing fluid flow rates of the respective phases, changing the relative viscosity or channel widths altogether[44]. More complicated dynamics may be achieved by heating the element[44].

2.2.2 Flow-focusing devices

Flow-focusing devices are defined by a narrowing of a microchannel to an orifice, which causes flow focusing, in turn causing an increased pressure and viscous stresses[43]. In this model, the disperse phase lies within a central channel aside two outside channels containing the continuous phase[43]. The phases mix by meeting at an orifice that subjects the disperse phase to symmetric shearing stresses, and ultimately produce a microdroplet through elongational flow in a repeatable and reliable fashion[50,51]. Elongational flow is governed by a pressure applied by the outer fluid and the viscous stresses within the inner disperse fluid, causing a strand that breaks at set intervals[44]. Unlike T-junctions, device synthesis in this manner is slightly more complicated, though also allowing for the construction of a number of different geometries. Flow-focusing devices are governed by a similar set of properties to that of the T-junction, namely channel geometry, flow rate, and viscosity[44]. The position at which the elongated strand breaks and forms a droplet is defined largely by the capillary number of the fluid system[44]. However, unlike the T-Junction, the droplet size varies with respect to the interfacial tension such that it can be significantly altered by the addition of surfactants, which change fluid surface tension[44]. As elucidated in two examples below, channel geometry may be altered in terms of reference to the central capillary.

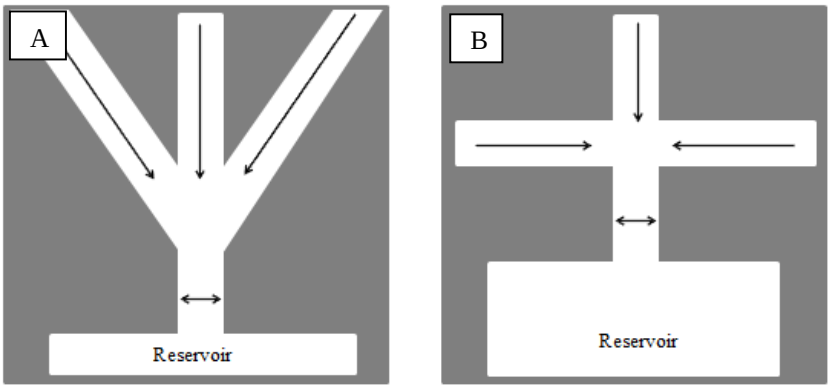

Figure 3: A depiction of a two flow-focusing geometries, (A) an angular geometry that facilitates increased shear stress on the middle, dispersed phase capillary and (B) a more elementary geometry with dual perpendicular entry of the continuous phase.

2.3 Simulations of microdroplet formation devices:

Simulations of MFDGs require a detailed incorporation of the physical laws that govern

laminar flow with immiscible fluids. For ease, these models will all be described on the basis of the COMSOL Multiphysics platform. Modeling in this manner remains important not only in the context of understanding and synthesizing the mechanical principles, but by avoiding potential losses in faulty fabrication. The simplest computer models in microfluidic droplet formation are those conducted in two dimensions with a geometry dominated flow device. In COMSOL Multiphysics, this may be accomplished via implementation of one of two methods: the application of the laminar two-phase flow, phase field module, conducted by Conhouso et al., or the conservative form of the level-set method, conducted by Nandakumar et al.

2.3.1 Laminar two-phase flow, phase field method in COMSOL Multiphysics

This laminar model relies upon a characteristic laminar flow that is readily attained by calculation of the Reynolds's number by Equation 1. In the phase field method, multiphase flow is a natural selection due to the presence of the continuous phase and dispersed phase. In COMSOL Multiphysics, a model parameter ϕ describes the disperse phase as $\phi = 1$ and the continuous phase as $\phi = 0$ with some middle value defining the species interface[41]. The conservation of mass equation or continuity equation is manipulated for incompressible flow such that[49]:

$$\nabla * \mathrm{u} = 0 \tag{5}$$

Here, u represents the velocity vector of either the continuous or disperse phase[1]. Likewise, the incompressible form of the Navier-Stokes Equation for the conservation of momentum is solved such that:

$$\rho\left(\frac{\partial u}{\partial t} + (u * \nabla)u\right) = \nabla * [-pI + \mu(\nabla u + \nabla u^T)] + F_g + F_{st} + F_e \tag{6}$$

In this case, p represents the pressure, μ acts as the dynamic viscosity, ρ as the fluid density, and F as the force vector for gravity, surface tension, and external forces respectively. Following Equation 5, this simplifies to:

$$\rho\left(\frac{\partial u}{\partial t} + u * \nabla u\right) = -\nabla p + \mu\nabla^2 u + F_g + F_{st} + F_e \quad (7)$$

Lastly, COMSOL Multiphysics applies phase flow by the incorporation of tracking parameters that describe energy transfer within the system[56]. The mixing energy in phase flow is defined in laminar phase theory by the incorporation of the aforementioned phase parameter ϕ and its relation to free energy as explored in more detail in Shen et al[56]. The result of their analysis leads to a manipulation of the Cahn-Hilliard equation, which describes the processes of separation of one or more phases[56]:

$$\frac{\partial \phi}{\partial t} + u * \nabla\phi = \nabla * \frac{\gamma^\lambda}{\epsilon}\nabla\psi \quad (8)$$

Here, λ is the mixing energy or energy density parameter, ϵ is the capillary width, γ is the so-called mobility, taken to be constant, and $\nabla\psi$ is defined[56]:

$$\frac{\delta F_{mix}}{\delta\phi} = \nabla\psi \quad (9)$$

Such that F_{mix} is the force of mixing. Equation 9 may be further manipulated such that a matching condition for the interfacial surface tension σ [41,56,57]:

$$\sigma = 2\sqrt{2} * \frac{\lambda}{3\epsilon} \quad (10)$$

Again, here λ represents the mixing energy density and ϵ is the capillary length[41]. In Couhouso et al. incorporation of these equations allowed for the simulation of several different flow rates and oil to water flow rate ratios at 15, 30, and 60 $\mu L/min$ and 1:1, 1:1.5, and 1:2, respectively[41]. This relatively simple simulation allowed for the determination of the effects on droplet diameter and frequency generation in terms of varied flow conditions. Such is demonstrated as a consequence of the capillary number, which is defined as:

$$Ca = \mu * \frac{N}{\sigma} \quad (11)$$

With all variables previously defined, the capillary number effectively describes the balance between viscous forces and interfacial forces within both the disperse and the continuous phases of this system[41]. At higher capillary numbers, generated droplets were observed to maintain a significantly smaller diameter due to increased shearing forces and likewise the frequency of droplet generation was found to be directly dependent on total flow rate[41]. A parametric analysis of this nature was also conducted by deMello et al., investigating the effects of both oil and water velocities on droplet formation within a flow-focusing droplet generator[58]. Alternatively, this study included experiments with high oil to water flow rate ratios confirming that the velocity ratio of the two phases directly determines the diameter of the droplets. Conclusively, a further study by Couhouso et al. applied this strategy to a number of geometries of flow-focusing devices observing that a wide and shallow rectangular geometry is preferred for uniformity over trapezoidal or narrow rectangular geometries[59].

2.3.2 Laminar two-phase flow, level-set method in COMSOL Multiphysics

As with the previous method, the level-set method demands that the fluids be well within the constraints of laminar flow. The level set method itself is a broad numerical analysis of shapes and figures that differentiates between topographical features and is often applied to analysis of complex Hele-Shaw Flows[44]. The level-set equation in this manner is defined as follows[60]:

$$\frac{\partial \phi}{\partial t} + \vec{u} * \nabla \phi = \gamma \nabla * \left(\epsilon \nabla \phi - \phi(1-\phi) * \frac{\nabla \phi}{|\nabla \phi|} \right) \tag{12}$$

Here, the level-set function ϕ defines the interface such that ϕ ranges from 0 to 1, similar to the phase field however any $\phi < 0.5$ corresponds to phase 1 and any $\phi > 0.5$ corresponds to phase 2 [54,60]. Likewise, γ determines the amount of reinitialization of the level-set function with suitable values comparable to the maximum value of the velocity field $\vec{u}$ [54,60]. Lastly, ϵ is proportional to the thickness of the transition layer[60]. Surface tension may be calculated by manipulation of the unit normal vector to the interface and the curvature, respectively (19).

$$\hat{n} = \frac{\nabla \phi}{|\nabla \phi|} \tag{13}$$

$$\kappa = -\nabla * \hat{n}|_{\phi=0.5} \tag{14}$$

$$F_{SF} = \sigma\kappa\hat{n}\delta \tag{15}$$

The σ above represents the interfacial tension coefficient and δ is the Dirac delta function that is only nonzero at the fluid interface[44,60].

$$\delta = 6|\nabla\phi| * |\phi(1-\phi)| \tag{16}$$

Finally, Equations 12 through 15 may be incorporated with the incompressible Navier-Stokes equation[50]. These functions are readily available in COMSOL Multiphysics and can be manipulated simply upon entry of the physical parameters above. Though applied to an "inkjet model", the figures below are largely applicable to the class of flow-focusing droplet generators with the exception that the center capillary must be divided into three separate channels as depicted in Figure 4A[60].

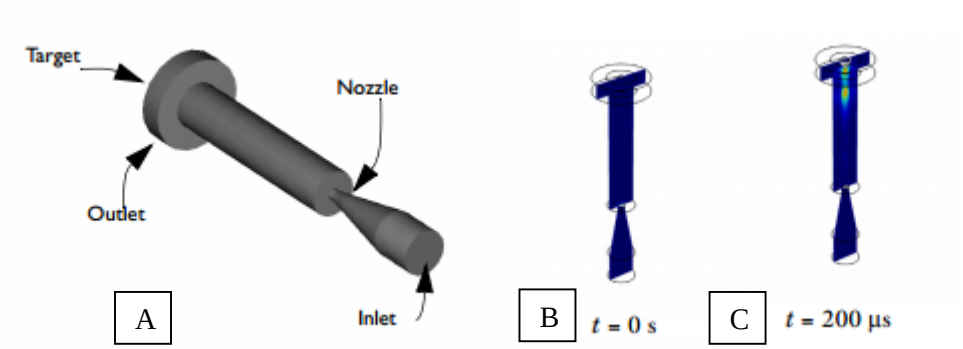

Figure 4: In the ink jet model (A), ink is injected through an inlet and follows out of a constricted nozzle that allows for a drop formation shortly after t = 0 s (B) that eventually hits a target near the outlet (C). The model maintains symmetry around the central axis.

This model was extrapolated to a flow-focusing MFDG by Nandakumar et al. as a means of determining the mono-dispersed and poly-dispersed droplet breaking processes by varying the viscosity of the disperse phase[60]. The fundamentals of this model included flow through a contraction, similar to Figure 4A, but with a continuous phase injected from two side

channels[60].

Simulation results qualitatively matched those of experimental findings with mono-dispersed breakup observed at low disperse phase viscosity and low capillary number[60]. These trends prompted the identification of two key fluidic regimes[61]. The squeezing regime is observed when the disperse phase blocks the entire capillary interface causing a pressure gradient and allowing for large droplet production[61]. A second phase, the dripping regime, is observed when the disperse phase does not block the entire capillary interface, therefore prompting the production of smaller droplets[61]. Satellite droplets are also observed in this regime above a certain flow rate of the disperse phase, which for the purpose of practical applications are particularly undesirable. Following the identification of these regimes, Nadakumar et al. concluded droplet size could be tailored primarily by controlling the orifice width and thereby the shear force exerted on the disperse phase[61]. Likewise, lower flow rates in this model parallel that of the phase field in that increased flow rate significantly reduced droplet size[61]. Thus this method effectively complements that of the phase field method in COMSOL Multiphysics while also elucidating mechanisms or regimes of droplet formation.

2.4 Practical applications of MFDGs

A number of unique technical platforms for MFDGs have been discussed both in terms of their developmental strategies and their relevant computer simulated models. Their development and assessment in this manner allows for application to a wide range of chemical and biochemical processes, the most essential of which pertain to, for example, biomedical advancement, protein crystallization, and chemical kinetics. Subsequently, the industrial application of droplet microfluidics remains pertinent to bioreactor development and chemical reactions by which they offer a characteristically high level of process control and general sensitivity[62].

In terms of pertinence to microbial communities, droplet generation in this manner allows for a large scale study of microbial interactions crucial for the survival of such communities and may be pertinent to the development of algal byproducts like synthetic fuels, cosmetics, and so forth[66]. This approach is unique in that most laboratory experiments are designed around purified samples of a single species, a phenomenon markedly rare in nature, suggesting an unknown network of mutualistic or communalistic relationships[66].

The approach for the creation of these microbial communities is also a paradigm of T-junction MFDG implementation, which is depicted below with permission of Nina Lin of the University of Michigan – Ann Arbor.

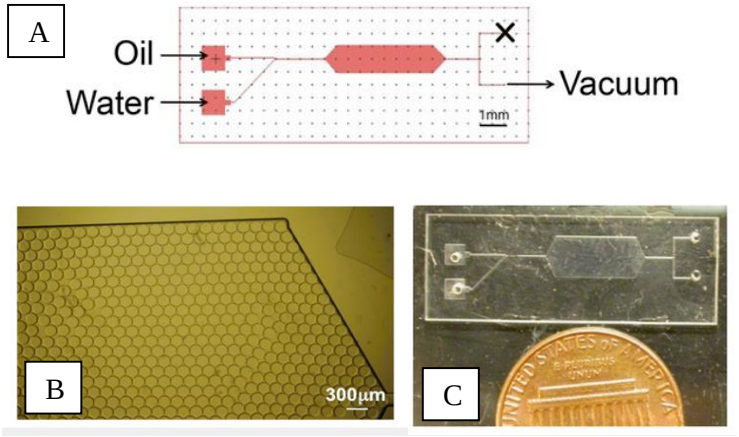

Figure 5: (A) The schematic for the slanted T-junction allows for the introduction of the continuous phase with algae such that (B) a large number of droplets of uniform diameter are produced. Also visible is the minute size of the entire construction in (C).

This platform has been implemented to successfully demonstrate cross-feeding of two *E. coli* autotrophs which were tunable on the basis of certain gene regulation for amino acid synthesis[66]. It was upon this previous research and platform development that this algae microdroplet experiment was grounded.

2.5 Conclusions

This chapter provides a relatively comprehensive review of microfluidic droplet generators, simulation in COMSOL Multiphysics to elucidate the fluid mechanical principles at work, and a plethora of applications. The integration of MFDGs with complex modern diagnostic strategies offers great potential for revolutionizing the industry. Likewise, the range of simulations, geometries, and parameters as discussed concludes that droplets remain easily tailorable to experimental design, facilitating the capture of large and precise datasets. Further research could realize the development of robust lab-on-a-chip type designs that function as bioassays for point of care medical treatment, bioreactors for industry, or elements in discerning mechanisms of chemical synthesis and kinetics. Such developments will serve as a platform for further scientific advancement.

Chapter 3: A study of model microalgae communities in flask cultures

3.1 Initial species selection

The purpose of the initial flask experiment was to determine overyielding species under the conditions in our laboratory without media exchange. Liquid exchange in droplets is a commonly problematic field in microfluidics, with many experiments limited by evaporative losses when using microliter quantities. Furthermore, overyielding combinations under these conditions may deviate substantially from those elucidated in the literature. Initial strain selection stemmed from collaboration with Professor Bradley Cardinale's laboratory at the University of Michigan, which had previously commenced a number of microcosm and mesocosm experiments in BOLD 3N media, but with nutrient exchange. This laid an initial groundwork for narrowing species selection to those with a propensity to transgressively overyield within given combinations. The total list of species is available in appendix Table A.1. The species chosen to be used in this experiment are listed and labeled as follows:

Table 2: List of algal species and corresponding letter codes

Strain Name	**Letter Code**
Ankistrodesmus falcatus	A
Chlorella sorokiniana	C
Selenastrum minutum	E
Pediastrum duplex	G
Scenedesmus acuminatus	I
Scenedesmus ecornis	J
Selenastrum capricornutum.	L

An important caveat is that these species were chosen because they had indicated transgressive overyielding within specific culture combinations. Transgressive overyielding may be dictated in three central ways: ratio of biculture biomass with respect to average monoculture biomass (TO_{ave}), the ratio of biculture biomass with respect to the most productive monoculture within the combination (TO_c), and the ratio of the biculture biomass with respect to the most productive monoculture within the entirety of the experiment

(TO_{total}) as follows:

$$TO_x = \ln\left(\frac{B_{bi}}{B_{mono}}\right) \quad (16)$$

In Equation 16, categorization of B_{mono} will change the basis of the overyielding. Given that the purpose of the flask experiment was to replicate the results from Professor Cardinale's laboratory, all overyielding calculations were conducted with respect to most productive monoculture within the combination. Henceforth all considerations of transgressive overyielding will be discussed in the context of algal combinations.

3.2 Design of flask experiment

Initial culturing of algal species involved the careful selection of algal media and experimental design. Most algal species vary in their idealized medium and, accordingly, a number of generic medias are of importance. These mediums include Tris-Acetate-Phosphate (TAP), BG-11, and BOLD 3N for freshwater species and artificial seawater, enriched seawater, and F/2 mediums are incorporated for saltwater species[68]. A more exhaustive list and relevant recipes are provided on the Culture Collection of Algae at The University of Texas at Austin[68]. For continuity, this experiment was conducted using BOLD 3N liquid medium, a modification of Bold's recipe with general application to freshwater xenic microalgal cultures[69]. The contents of BOLD 3N media includes 8.82 mM $NaNO_3$, 0.17 mM $CaCl_2*H_2O$, 0.30 mM $MgSO_4*7H_2O$, 0.43 mM K_2HPO_4, 1.29 mM KH_2PO_4, 0.49 mM NaCl, and a P-IV metal solution containing 2.01 mM $NA_2EDTA*2H_2O$, 0.36 mM $FeCl_3*6H_2O$, 0.21 mM $MnCl_2*4H_2O$, 0.037 mM $ZnCl_2$, 0.0084 mM $CoCl_2*6H_2O$, and 0.017 mM $Na_2MoO_4*2H_2O$. Of these, the most important for algal growth appear as sodium nitrate and potassium phosphate for the quintessential sources of nitrogen and phosphorus.

Algal bicultures and monocultures were to be incubated in a repurposed refrigerator maintaining a temperature of approximately 25^oC, with variations due to convective differences between the thermometer at the top of the fridge and cooling unit at the base. Shakers were fitted with wooden platforms and grip liner to increase friction between the flask and platform interface. The platform was designed to fit approximately one hundred glass 125 mL flasks on two shakers with two sets of light fixtures. Based on closeness to resembling

sunlight, Philips 280933 – F17/Tl830/Plus/Alto Straight T8 Fluorescent Tube Light Bulbs characterized by a luminous flux of 1375 lumens, a color rendering index of 85, and a color temperature of 3000K [70]. Culturing was conducted in Pyrex 125 mL flasks with a volume of 50 mL autoclaved BOLD 3N per flask to ensure adequate growth.

Experiments were conducted in quadruplicate to ensure accurate results such that, given the six species of interest, total flask demand was calculated combinatorically indicating 84 flasks. Given the space constraints, *Scenedesmus ecornis* was added with a *Selenastrum minutum* biculture, which indicated promising preliminary results and subsequently a total of 92 flasks. Targeted flask inoculations were $1.0 * 10^4$ cells/mL, accomplished by sonicating, reading with a hemocytometer, and then inoculating fresh media to a desired concentration. Sonication was quintessential as certain species like *A. falcatus* and *P. duplex* were prone to flocculation, posing a particular challenge to cell counting. Flasks were inoculated in a biosafety cabinet and resealed with sterile aluminum foil. No CO_2 feed was used such that the algae were limited to environmental CO_2 concentrations.

Inoculated flasks were then loaded onto the shakers at random to mitigate environmental variability within the fridge. Flasks were read daily with $200\ \mu L$ algal samples in Greiner black 96 well plates using a Spectramax M5 plate reader paired with Softmax Pro 5.3 software. Microalgae have specific biochemicals that fluorescence at different wavelengths, specifically chlorophyll-a, chlorophyll-b, and carotenoids, which make up the major pigments within plants and algae. These are commonly used as proxies for growth and biomass accumulation due to their essentiality for photosynthesis and plant metabolism and, likewise, biomass measurements become increasingly difficult at small scales. In accordance with chlorophyll-a fluorescence, plate reading parameters were set to an absorbance of 465 nm, which is blue light, and an emission of 665 nm.

Every five days $1.0\ mL$ of fresh BOLD 3N media was added to each flask to ensure a stable volume over the growth period. Combined, these readings facilitate the determination of algal growth rates and carrying capacity upon reaching a steady, stationary phase. A plot of biomass accumulation with respect to time is indicated in Figure 6.

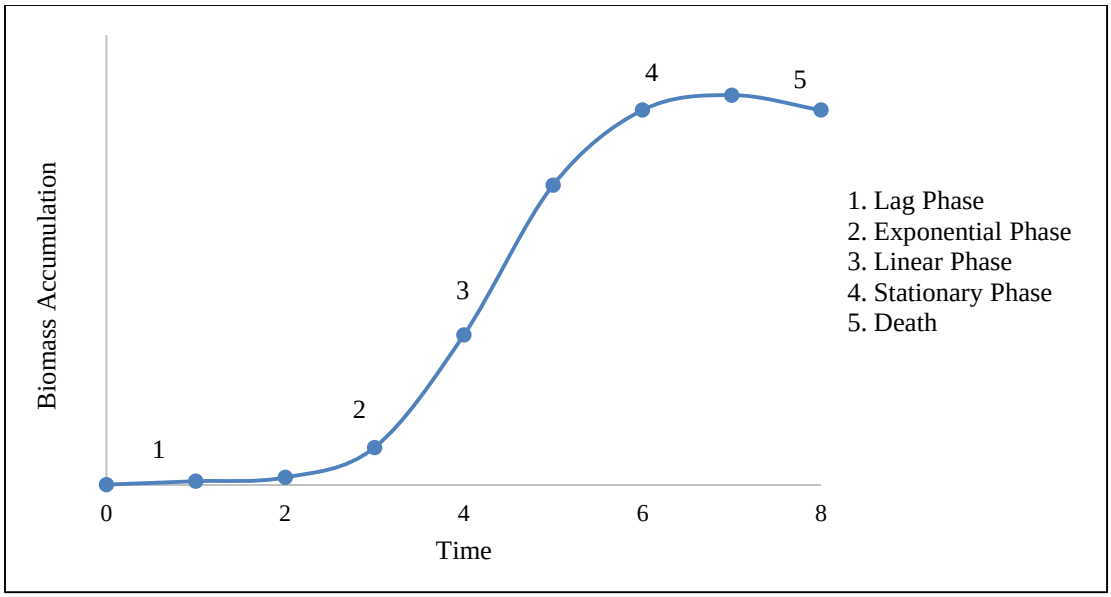

Figure 6: Ideal depiction of algal logistic growth phases in batch culture (no medium exchange)

Likewise, this growth period was closely monitored for each culture such that the culture was deemed in stationary phase and removed from the system after decreasing for more than 3 days. This was conducted primarily to avoid the characteristic overshoot of particularly fast growing algal species, which could adversely affect estimates of growth rate and carrying capacity. Algae were again studied under hemocytometer to ensure the absence of contamination and, given cleanliness, were vortexed, centrifuged in preweighted $50\ mL$ Fisher conical, and dried for three days at $60^{o}C$ in an oven to facilitate dry biomass comparisons. Alternative attempts at drying the biomass included a Kimble-Chase vacuum manifold assembly with Whatman filter paper, though media waste throughput indicated incomplete separation of the suspended algae from the media. Several flasks were also excluded from analysis due to torn aluminum foil, which likely increased gas exchange within the flask and surrounding environment. Control conicals were also used to account for vapor losses from humidity changes. This value was subtracted from all conicals prior to biomass and overyielding calculations. These calculations were carried out using standard error propagation.

3.3 Results from flask experiment

Biomass measurements were collected for each biculture and monoculture after attaining their estimated carrying capacity. This allowed not only for comparison of biomass

accumulation between monocultures and bicultures, but for estimations of their relative growth rates and carrying capacities. Biomass results indicated the dominance of *P. duplex* and *S. capricornutum* in terms of total biomass generation in monoculture as well as trends within biculture combinations. Of the seven monocultures explored, *S. ecornis* and *S. minutum* indicated the least endpoint biomass. These biomass measurements in mg per conical are indicated in Figure 7:

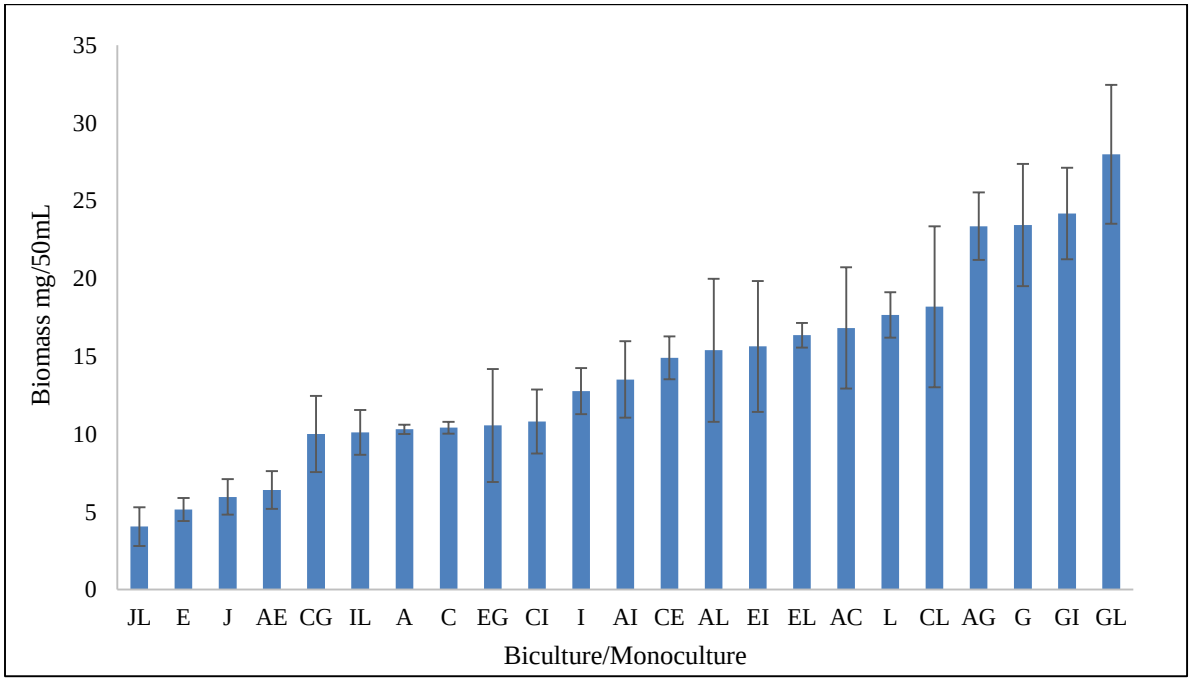

Figure 7: Biomass per conical after attainment of steady state

Microscopic study of bicultures via hemocytometer also allowed for the estimation of endpoint species ratios between those with significantly different morphology. Two important trends include the near dominance of *C. sorokiniana* in bicultures as well as the apparent absence of *P. duplex* in bicultures. In the "GI" and "CG" bicultures, for example, *P. duplex* was seemingly absent. This apparent paradox may be largely attributed to flocculation and the natural formation of algal coenobia, a characteristic native to the *Pediastrum* genus amoung others[71]. The variance of size and formation of coenobia makes cell counting particularly troublesome even despite vigorous vortexing and sonication. On the other hand, "CI" and "AC" had cell ratios of 8:1 and 1:20, respectively.

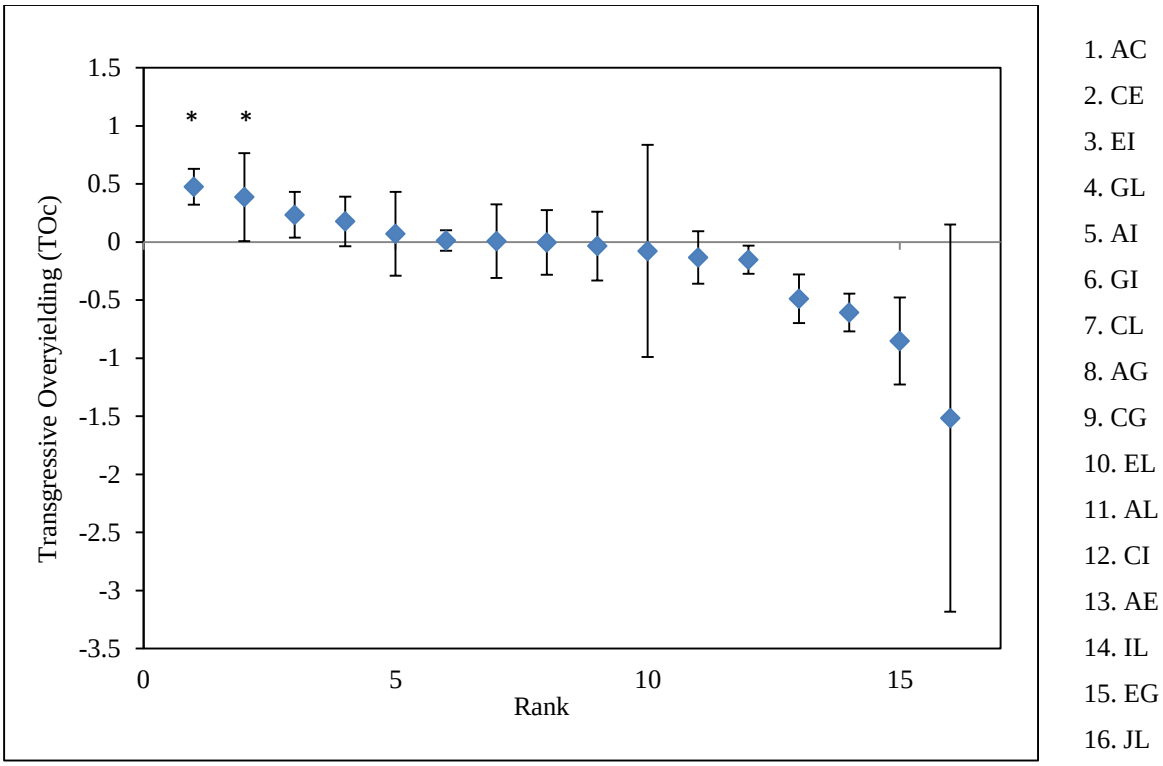

Figure 8: Analysis of Transgressive Overyielding (TO_c) in BOLD 3N media

Of the species listed in Figure 8, six species combinations demonstrated some degree of transgressive overyielding with two combinations being statistically significant. These species combinations were particularly important for translation into a microfluidic droplet generation device. An important aside is that these combinations do not necessarily reflect those with the greatest biomass generation, rather those that have the highest transgressive overyielding within the given combination. In microdroplets, the combinations with the highest propensity for transgressive overyielding would be the targets for study to determine whether variables in microdroplets (change in carrying capacity, mass transfer, etc) had significant effect on cultures. These were calculated for significance using a one-tailed Student's T-Test. Explicitly, the top four combinations were *A. falcatus* and *C. sorokiniana* (p= 0.016), *C. sorokiniana* and *S. minutum* (p=0.0013), *S. minutum* and *S. acuminatus* (p=0.11), and *P. duplex* and *S. capricorntum* (p=0.10). Ranks 12 through 16 demonstrated statistically significant transgressive underyielding. Fluorescence readings over the period of approximately 45 days allowed for the determination of individual carrying capacities and growth rates for each culture through application of the Verhulst logistic growth model. This was easily translatable to the MATLAB curve fitting application using the boundary conditions of initial fluorescence

with data sheets uploaded from Microsoft Excel. The formulas used were as follows:

$$N(t) = \frac{K * N_0}{(K - N_0) * e^{-rt} + N_0} \tag{17}$$

$$N(0) = N_0 \tag{18}$$

This MATLAB utility also supplied confidence intervals as indicated in Figure 9 for the monoculture *S. minutum*, where M represents the relative fluorescence units of the M5 spectrophotometer:

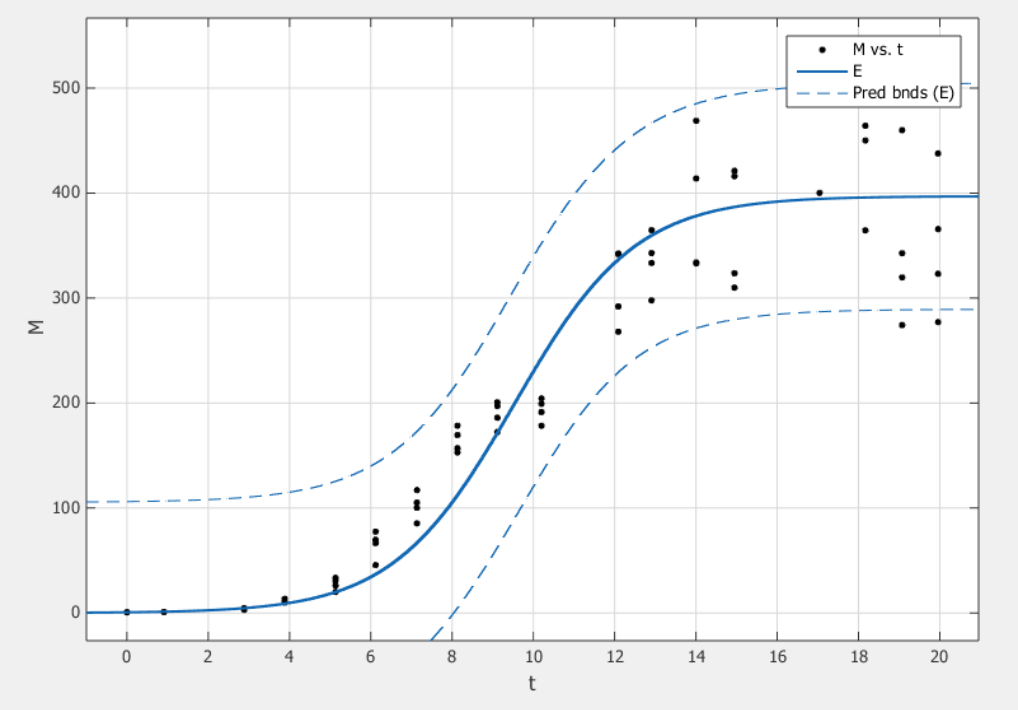

Figure 9: MATLAB curve fitting of *S. minutum* with 95% CI's

This analysis was conducted for all monocultures and polycultures and then the derived carrying capacity was used to recalculate transgressive overyielding. A full table of growth rates, carrying capacities, and statistical analyses of the logistic curves is presented in appendix Figure A.1.

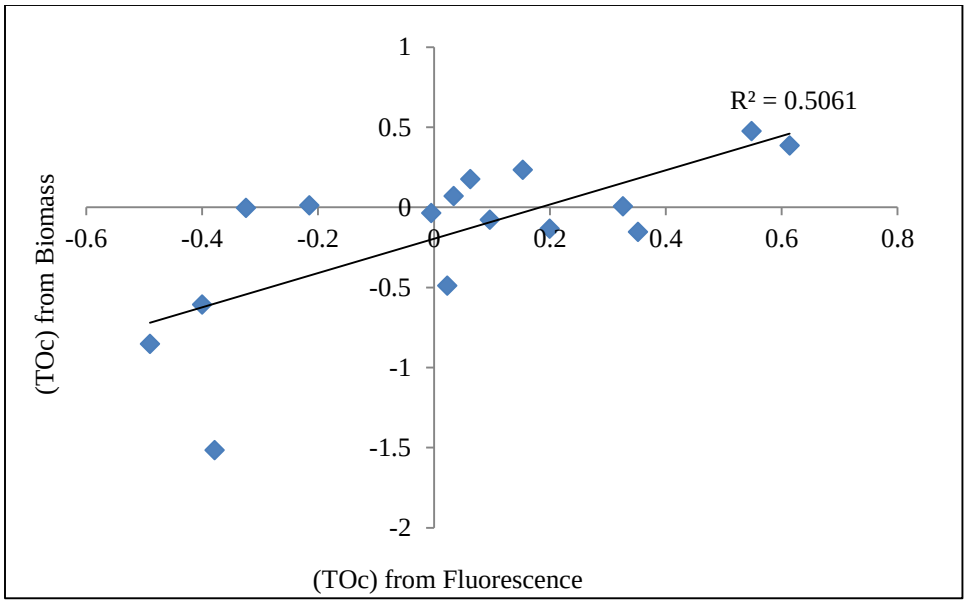

Figure 10: Comparison of transgressive overyielding on carrying capacity estimated from fluorescence curve fitting and that from end-point biomass measurement

While an R-squared of 0.5061 as indicated in Figure 10 is certainly lower than anticipated, an important observation is that this comparison tends to discriminate in favor of biomass overyielding, suggesting that the proxy, fluorescence, is a more vigorous criterion. A second observation is that the R-squared value for overyielding exclusively from monocultures yields a value of $R^2 = 0.8662$, as indicated in appendix Figure A.2. This juxtaposition suggests that the nature of bicultures contributes non-logistically. One explanation is that species have differing growth rates leading to a bimodal character. Mathematical modeling of communities has been well explored by Lotka and Volterra, though facilitative relationships remain particularly difficult to model due to limitations by density-dependence rather than competitive interactions.

Chapter 4: Droplet cultivation of model microalgae communities

4.1 Criteria for droplet generation

While the previous chapter was successful in indicating transgressive overyielding relationships between multiple species of algae, it also provided a brief depiction of the amount of resources, space, and time necessary to grow algal combinations. The purpose of employing microfluidics in this case is to establish a high throughput mechanism for the timely screening of many combinations of algal polycultures. Screening all combinations within the seven species demands 65 cultures excluding replicates. Again considering the range of algal species available for screening beyond these explored in this study, screening could involve greater than 10^6 combinations, a number that is simply not realistic in bench sized laboratory experiments on the grounds of both cost and time. Microfluidics offers a unique opportunity for screening capabilities. However, in order to translate the characteristics from the flask experiment to microdroplets, several fundamental principles must be considered:

1. **Sustained Storage:** Droplets must maintain integrity and a majority of initial volume over algal growth cycle, estimated to be approximately 20 days.
2. **Uniformity:** Droplets must be generated uniformly with a relatively low polydispersity index and maintain said uniformity over the course of the experiment.
3. **Swift Analysis:** The high throughput nature of this experiment demands an analysis framework that is straightforward, quick, and user friendly.

These design criteria were fundamental in selection of the polymer as well as the microfabrication pathway.

4.2 Microfabrication of poly(dimethylsiloxane) device via photolithography

Development of microfluidic devices has been well explored within the last several decades as perhaps most popularized by George M. Whitesides at Harvard, who established PDMS fabrication via photolithography for rapid prototyping[72]. From this framework, designs may be quickly crafted using computer aided design (CAD) software and, within 24 hours, translated into an applicable device. This MFDG was designed using PDMS largely due to the ease of fabrication pathway and relative cost with respect to alternatives, which include glass,

polymethyl methacrylate, paraylene, and polystyrene. While glass was employed in the microbial experiment conducted by *Park et al.*, this process requires wet etching with hydrofluoric acid as the etchant. Not only is this arguably the most dangerous commercial acid, but wet etching demands a significant investment in cleanroom laboratory training. PDMS is a silicon-based amorphous polymer with the repeating $(CH_3)_2SiO$ monomer with optical transparency, biocompatibility, and temperature stability. Unlike glass, PDMS is relatively elastic depending on baking procedures and, more importantly, hydrophobic and gas permeable. This gas permeability has been considered essential for microbial droplet storage in PDMS as algae require gas exchange for growth.

This microfabrication strategy is described pictorially in Figure 11 below:

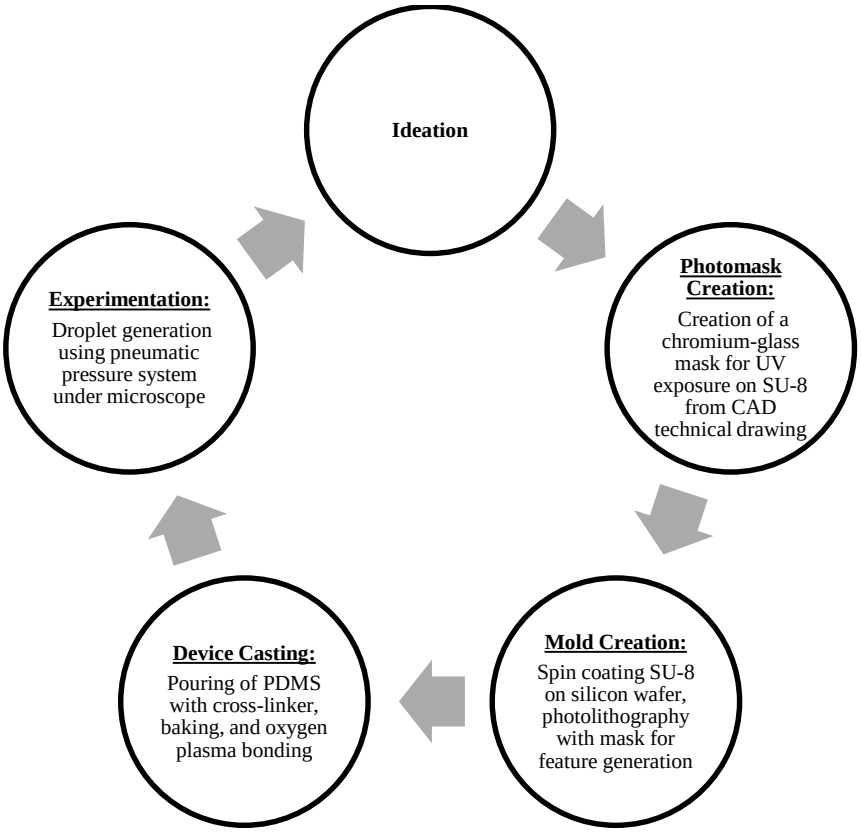

Figure 11: Rapid prototyping process for PDMS microfluidic devices

Initially, a CAD technical drawing was created using L-edit, a design program that is readily applicable to the Lurie Nanofabrication Facility at the University of Michigan. This design included a simple flow focusing device as typified by Figure 3B with an orifice opening of 50 μm and channel diameters of approximately 100 μm. These dimensions were selected

so generate $100\,\mu m$ diameter droplets. This design was readily translated to a Heiderlberg µPG 501 Mask Maker as a GDSII file andrun in high throughput writing mode using a chrome in glass substrate for the photomask, given the relative size of the features. SU-8 is a negative photoresist and thereby solidifies under UV exposure, this photomask was designed to match the intended PDMS layout.

Next, a SU-8 mold was developed using a silicon wafer using SU-8 2035 (MicroChem). The SU-8 2000 series has characteristic high aspect ratio imaging as well as a wide range for feature generation, which are ideal for this project. Photoresists within this series differ slightly in terms of their percentage of solids, which affects density and viscosity significantly. A spin coating protocol for a $50\,\mu m$ film thickness was used, specifying acceleration profiles according to SU-8 2035. Exposure was then carried out using a mask aligner in tandem with the photomask developed in the LNF. Given the UV dosage of $20 MJ/cm^2 s$ and, again, the criteria for SU-8 2035, the wafer was exposed for a total time of 10 seconds. The wafer was then baked and developed using SU-8 developer and subsequently washed with acetone and isobutyl alcohol. The complete process flow is supplied by MicroChem© and replicated in Figure 12 below[73]:

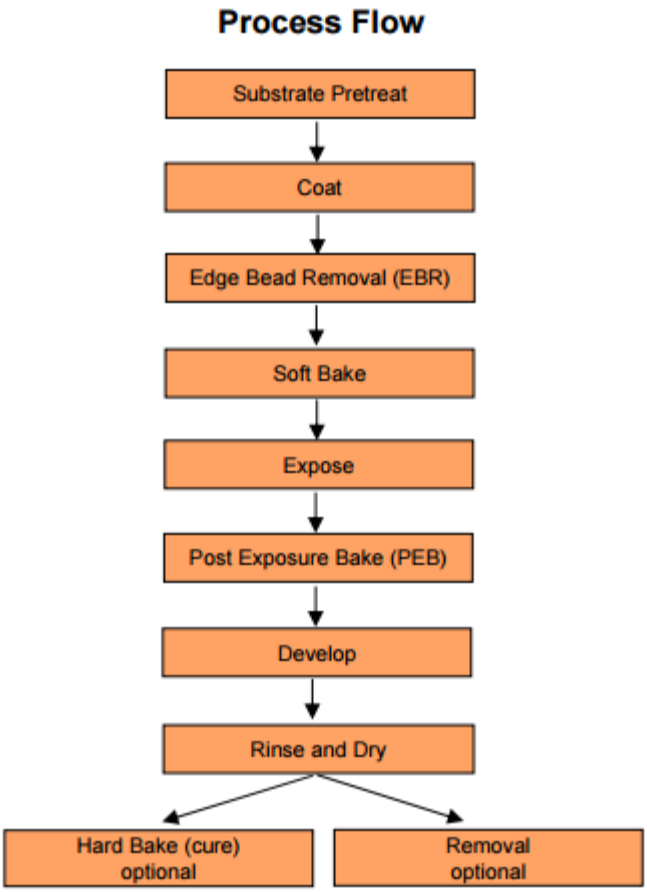

Figure 12: Process flow from MicroChem for SU-8 2000 series photoresists[73]

After developing, this photomask was treated with trichloro(1,1,2,2-perfluoocytl)silane in a vacuum chamber, a crucial step that leads to the formation of a monolayer on the silicon surface, reducing surface energy and increasing hydrophobicity[74].

The silicon mold and a blank silicon wafer were then washed with acetone and dried with nitrogen, the blank silicon wafer PDMS layer serves as a base for the features. For PDMS formation, these were placed in weigh dishes with a 10:1 w/w mixture of pre-polymer Slygard 184 from Dow Corning and cross-linker. Air was removed from the dishes using a vacuum pump for one hour followed by curing at $80^{o}C$ overnight. After baking, the PDMS was removed from both wafers and dishes, cut into manageable slabs with a razor blade, and cleaned with 3M Scotch tape. Three holes were punched through the PDMS feature layer in each device to facilitate insertion of 1.5mm PET tubing and syringes for future droplet generation. The base PDMS layer and featured PDMS layer were then bonded using plasma

treatment for ten seconds per device. A second set of devices was also generated using the same protocol, but instead of bonding to a secondary blank PDMS layer they were bonded to glass. Finally, both sets of devices were baked for 6 hours to further increase hydrophobicity prior to use in droplet generation.

4.3 Droplet generation of algal cultures

The droplet generation framework used for these experiments follows that explored by *Park et al.*, specifically in the set-up of multiple pneumatic pumps that use forced air in tandem with a voltage control through LabView programming. This set-up was designed at a microscope station equipped with a Nikon Eclipse Ti-S and Nikon Intensilight C-HGHI. Such equipment allowed for real time analysis not only of droplet generation but of fluorescence of chlorophyll-a within generated droplets. These pneumatic pumps were connected to a dual *2.5 mL* syringe system for the aqueous and continuous phases. The aqueous phase for these experiments involved BOLD 3N media as was used in the flask experiment, with the continuous phase consisting of 3M Novec HFE 7500 Engineered Fluid with a 2% wt 008-fluorosurfactant from RAN Biotechnologies. These syringes were then connected to PTFE microtubing with Norson precision tips designed for dispensing engineered fluid. The tips were then connected to a MFDG on a glass slide. The glass-PDMS contact was generally stable though, if necessary, sealed with epoxy.

The initial experiments using these devices were carried out using *C. sorokiniana*, which is morphologically convenient, easy to count, does not flocculate, and maintains a particularly fast growth rate as indicated in the previous flask experiment. Generation of encapsulated chemicals or microbes in droplets has been previously demonstrated to follow a Poisson distribution such that cell concentrations could be easily adjusted[66]:

$$P(X = k) = \frac{e^{-\lambda}\lambda^{k}}{k!} \tag{19}$$

Here, λ represents the expected number of events and k is the integer number of events in the interval. Bicultures will innately demand at least 2 cells per droplet such that this formula can be used to estimate cell density. Estimated droplet concentrations can also be calculated by extrapolating hemocytometer cell counts in terms of $cell/mL$ to $cells/droplet$ given the

estimated cell droplet formula provided by the depth of the MFDG, $50\mu m$ and the proposed droplet diameter,$100\mu m$, via the volume of a cylinder, indicating about $400\ pL$. This suggests a targeted initial density of approximately $5.1 * 10^6\ cells/mL$ for $\lambda = 2.0$, $2.6 * 10^6\ cells/mL$ for $\lambda = 1.0$ and so forth. It should be noted that these droplets are not actually cylinders and using this approximation inherently undershoots the actual distribution because the actual droplet volume will be slightly higher. Likewise, the uniformity criteria for droplet generation becomes increasingly important. If droplets have a high PDI, then deviation from the estimated lambda was assumed to vary considerably. To avoid deviation from the estimated droplet density, samples were sonicated for 5 minutes and vortexed for 30 seconds.

The storage mechanism for these droplets was designed to be readily integratable with the MFDG using a perforated, sterile 1.7 mL Eppendorf tube for insertion of a 1.5 mm diameter PFTE tubing and a Nordson precision tip, both of which sealed with Devcon Home H_2 Hold All-Purpose Epoxy. After generation, droplets were stored within the Eppendorf tube with the addition of generic mineral oil. As a less dense fluid, the mineral oil would provide an insulating layer above the microdroplets, which would in turn rest above excess oil used in droplet generation (Figure 13D).

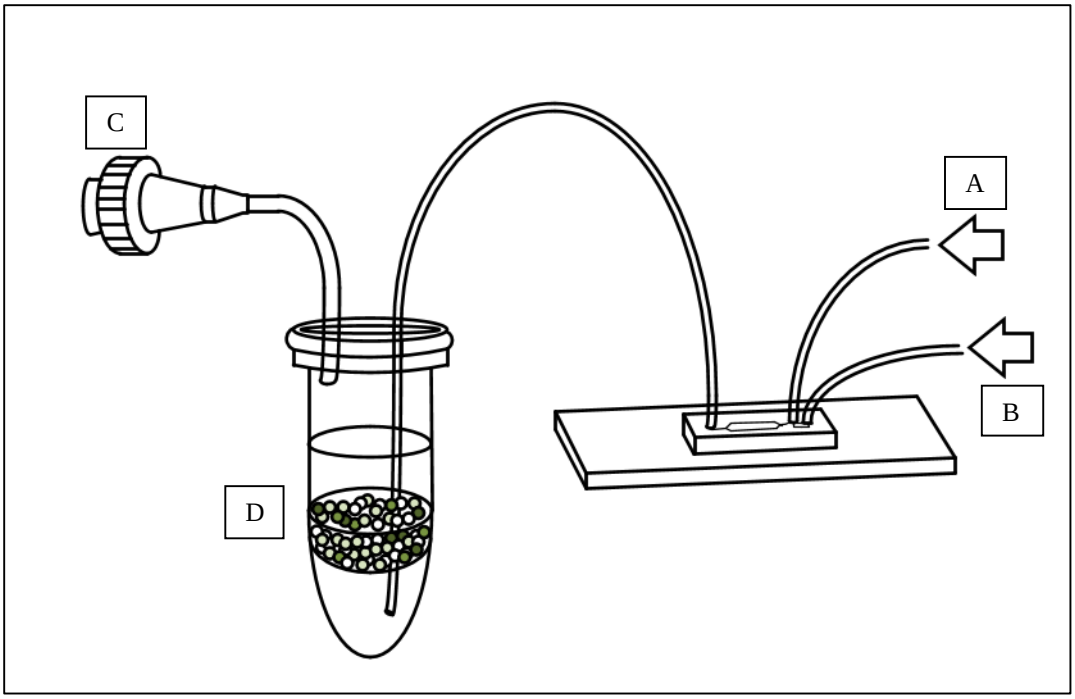

Figure 13: Design of Eppendorf storage unit with MFDG (**Not to scale**). (A) Aqueous phase of BOLD 3N media for droplet generation, (B) continuous phase of Novec HFE 7500 with surfactant, (C) syringe tip for pumping out droplets for future analysis, and (D) visualization of the three layers of mineral oil (top), droplets, and then excess continuous phase

For given point reads, these droplets could then be extracted and visualized on a disposable hemocytometers (iNCYTO C-Chip DNC-N01). This method allowed for a relatively sterile storage environment for bulk droplets. The ability to produce uniform droplets is epitomized in Figure 14.

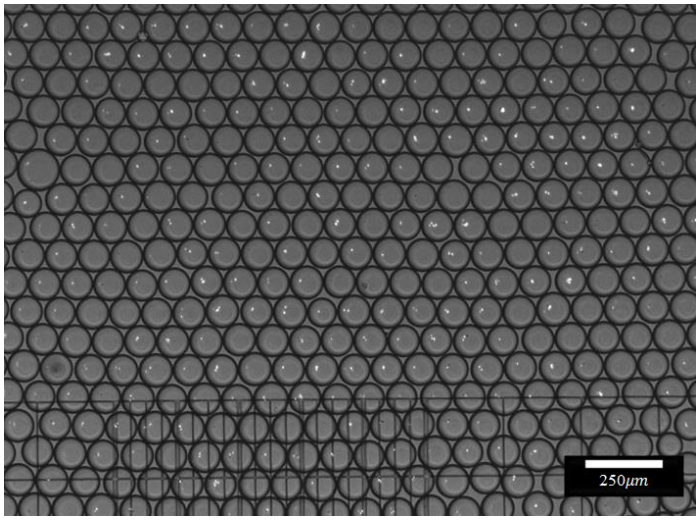

Figure 14: Monodispersed droplets of *C. sorokiniana* at day 0

After successful encapsulation of the monoculture in highly uniform droplets, this process was then repeated for the first biculture of interest: *A. falcatus* and *C. sorokiniana* to consider the proportion of droplet generation. Biculture feedstock was made by mixing both species together in a 1:1 ratio at a specified concentration. At $100\ \mu L$ volumes, the droplets are inherently heterogeneous such that some will have monocultures of *A. falcatus*, some with monocultures *C. sorokiniana*, and others as bicultures. The selected λ value must be large enough to facilitate the generation of all three, but not large enough to generate all bicultures.

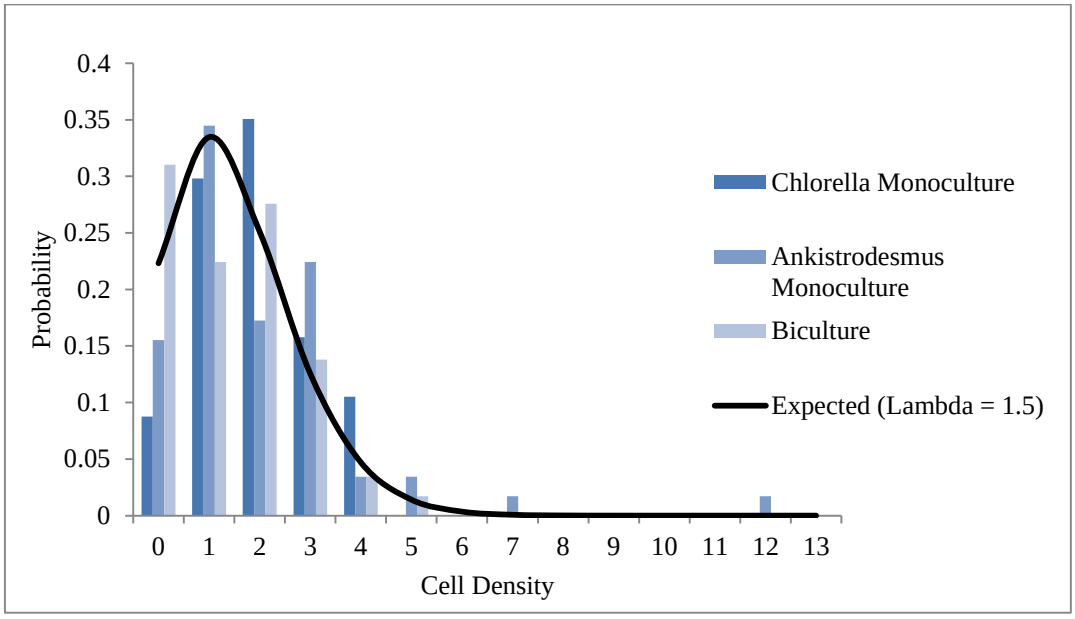

Figure 15: Poisson distribution of cells per droplet for *Ankistrodesmus falcatus* and *Chlorella sorokiniana* after droplet generation (n=50)

Qualitatively, Figure 15 indicates rough adherence to the estimated Poisson distribution with $\lambda = 1.5$. To obtain this value, the biculture feed was composed of equal portions of each algal strain. This method avoids the necessity of multiplying Poisson distributions that is necessary when combining two independent aqueous streams within the device[75]. Deviations from the expected proportions stem not only from the cylindrical approximation of droplet volume, but also from the inherent degree of heterogeneity within algal cultures. Even setting up the experiment could allow for algal settling within the precision tips, thereby producing a number of droplets with disproportionately high cell densities and subsequent droplets with subtly lower cell densities.

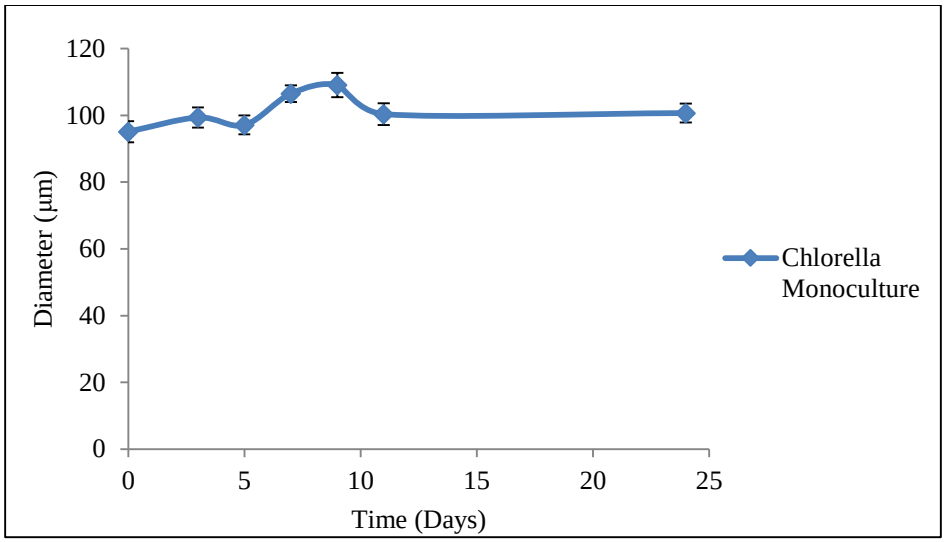

Figure 16: Droplet diameter of *C. sorokiniana* over 25 days

Likewise, experiments demonstrated droplet diameter consistency over the entire algal growth period as apparent in Figure 16.

4.4 Screening protocol for microdroplet overyielding

Images captured with the Nikon Eclipse Ti-S could be quickly taken and saved using the program QCapture 5.1, which has tunable settings for gain, format, and sampling length among others. These, in tandem with the microscope's bandpass filter wavelength, allow for quick comparison of bright field and fluorescent field images. These overlays were necessary for distinguishing cells and observing droplet boundaries. Images recorded in QCapture were then uploaded to Adobe Photoshop, where droplets could be individually identified and categorized based on composition, droplet diameter, and measurement time. A sample pool of approximately fifty droplets was taken at each reading with twenty droplets containing cells randomly selected from within that pool. The use of a hemocytometer for measurements means that each measurement studies a completely different population of droplets with the assumption of a similar overall population mean. The fact that individual droplets are not tracked over the experimental time period means that overall error will be substantially higher. Nonetheless this avoids the necessity of constructing a humidified environment in which a monolayer of droplets can be readily generated and stored over the growth periods. Previous attempts at constructing such a device were futile largely due to evaporative losses and

diffusion through the PDMS. While various papers have indicated that such a monolayer is indeed possible, their methods appear to necessitate a highly controlled environment with humidification equipment[76,77].

After identification in Adobe Photoshop, these droplets could be saved as .BMP files studied relatively quickly using ImageJ and a flexible forloop, which translated input images to 8-bit, set specified thresholds, and recorded a separate reading for each file. Readings from ImageJ provided the fluorescent intensity and fluorescent area for each droplet which, when multiplied, could be used to calculate an estimated total fluorescence of each droplet. This product is particularly important as area and intensity are nonlinear.

Likewise, there are a number of important factors that alter fluorescence measurements beyond droplet volume and were studied accordingly. These include the effects of gain on the fluorescent images recorded in QCapture, the platform distance, and clarity on total fluorescence. The threshold for fluorescence detection in ImageJ could also be manipulated to effect final fluorescence readings considerably. All of these factors were particularly important for sensitivity analysis, assuring the integrity of the image analysis process, and adequate optimization. Specific threshold and gain combinations could skew fluorescence readings considerably. Likewise, photoinhibition of algal cells could cause significant variation, demanding that a light source and photo be taken in quick succession.

4.5 Results from algal droplet cultivation

Of the overyielding combinations from Figure 8, two bicultures, *C. sorokiniana* and *S. minutum* (CE) and *A. falcatus* and *C. sorokiniana* (AC), were chosen as they indicated the largest transgressive overyielding. The biculture *S. ecornis* and *S. capricornutum* (JL) was also selected to analyze apparent negative relationships. Each biculture study consisted of three Eppendorfs, one with a biculture and two with its respective monocultures. These monocultures could then be used both as controls for comparison to the biculture. Theoretically, each experiment would only require a single mixture of monocultures and bicultures, however species combinations like CE are difficult to distinguish under the microscope at 10x magnification. Further magnification slows analysis considerably. Instead, these cultures would be lumped and compared to individual monocultures. Such an approximation inherently reduces the effects of transgressive overyielding and its validity was considered throughout the

experiment.

The biculture CE was chosen for the first experiments as neither species had previously demonstrated significant flocculation and both species could be grown relatively quickly. Following the assertions made in Section 4.4, species were analyzed for the effects of gain, threshold and fluorescence as a function of distance of the objective. The lattermost study was deemed important because of the suspension of algal cells in each droplet were not necessarily within the same spatial plane, meaning some algal cells would be out of focus, contributing to deviations in fluorescent intensity and area. Three droplets of *C. sorokiniana* were considered each with a variable number of cells, but roughly the same diameter.

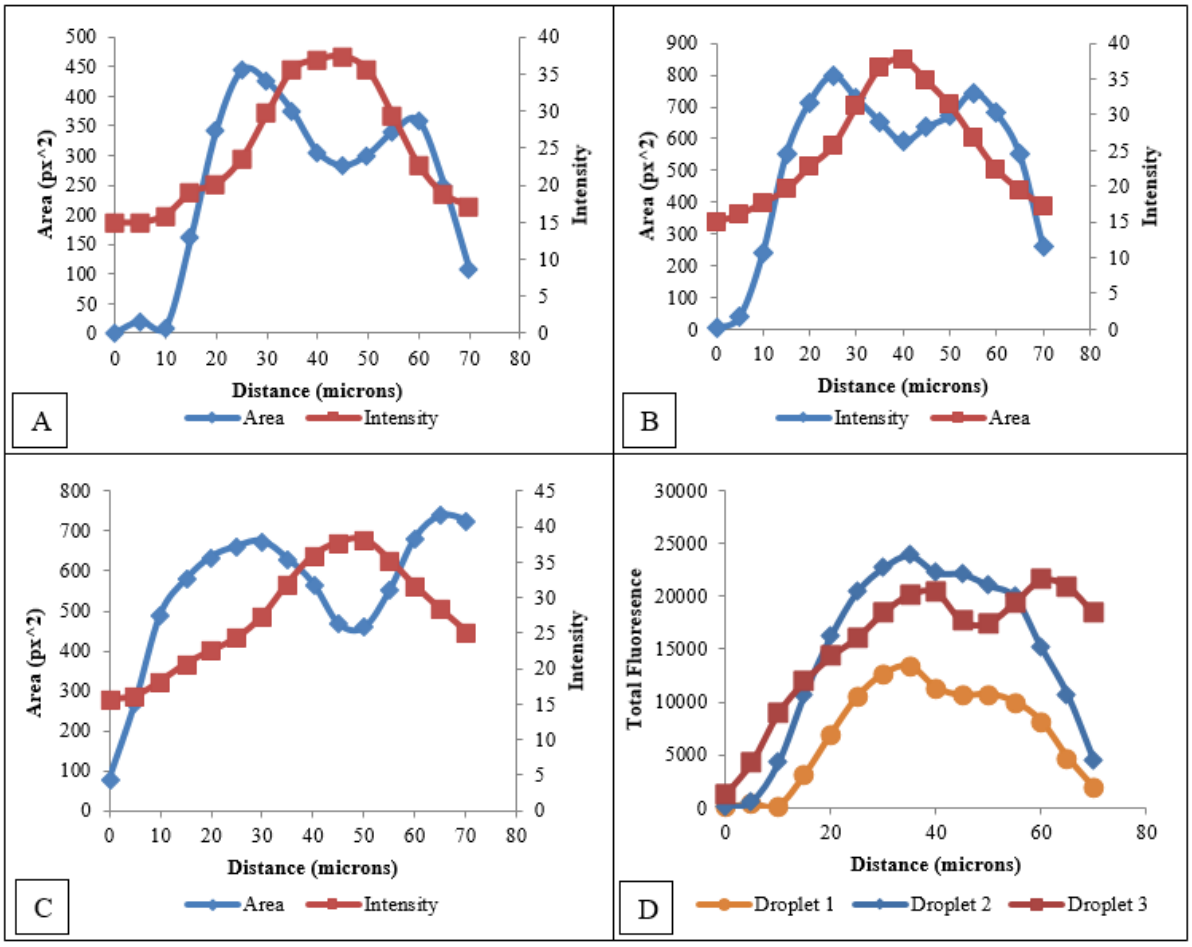

Figure 17: Effects of varying platform distance on fluorescence intensity and area. (A) Contained 8 cells, (B) contained 14 cells, (C) contained 11 cells, and (D) is a representation of all three droplets in terms of total fluorescence

This study concludes that while distance of the objective from the microscope lens varies both fluorescent intensity and fluorescent area, there is a range in which this difference is

relatively negligible due to their counteracting effects. This arises due to increased fluorescence when cells are in focus with an inversely proportional decrease in area. Similarly, intensity within *C. sorokiniana* and *S. minutum* was found to be relatively constant over the growth period of the algal droplets as indicated in Figure 18. This consistency is relatively important for the purpose of high throughput screening. If specific species of algae can be allocated to a specific range of fluorescent intensities within a finite range, polyculture droplet compositions might also be able to be estimated simply through intensity interpolation.

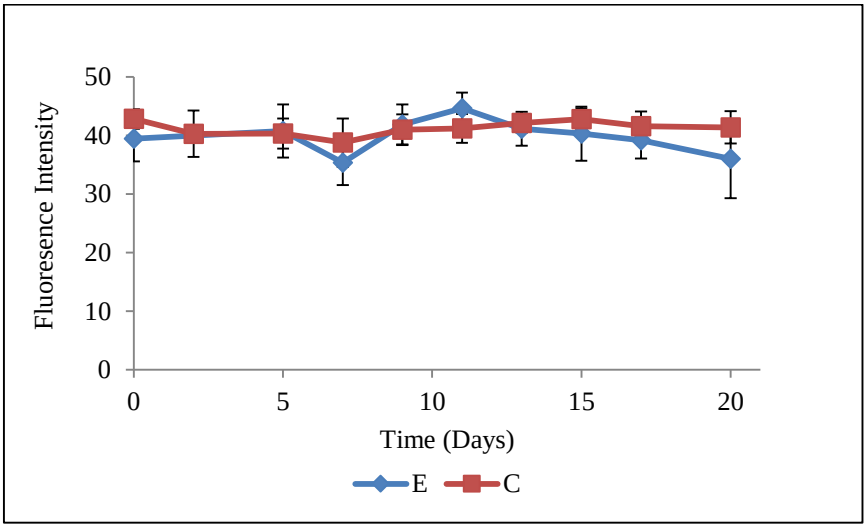

Figure 18: Fluorescence intensity from ImageJ for two monocultures of *C. sorokiniana* and *S. minutum* over a 20-day droplet growth period. Error bars indicate standard deviation.

Analysis of gains and thresholds were also considered within specific ranges. The threshold minimum was of particular relevance as a low threshold minimum boundary could wash out the images with too much fluorescence and a high threshold minimum boundary would reduce fluorescent area. These were studied with ranges from 4 to 14 and 1 to 3 for minimum threshold in ImageJ and gain in QCapture, respectively. It was found that gain and minimum threshold have linear effects on fluorescent intensity with coupled, nonlinear effects on fluorescent area.

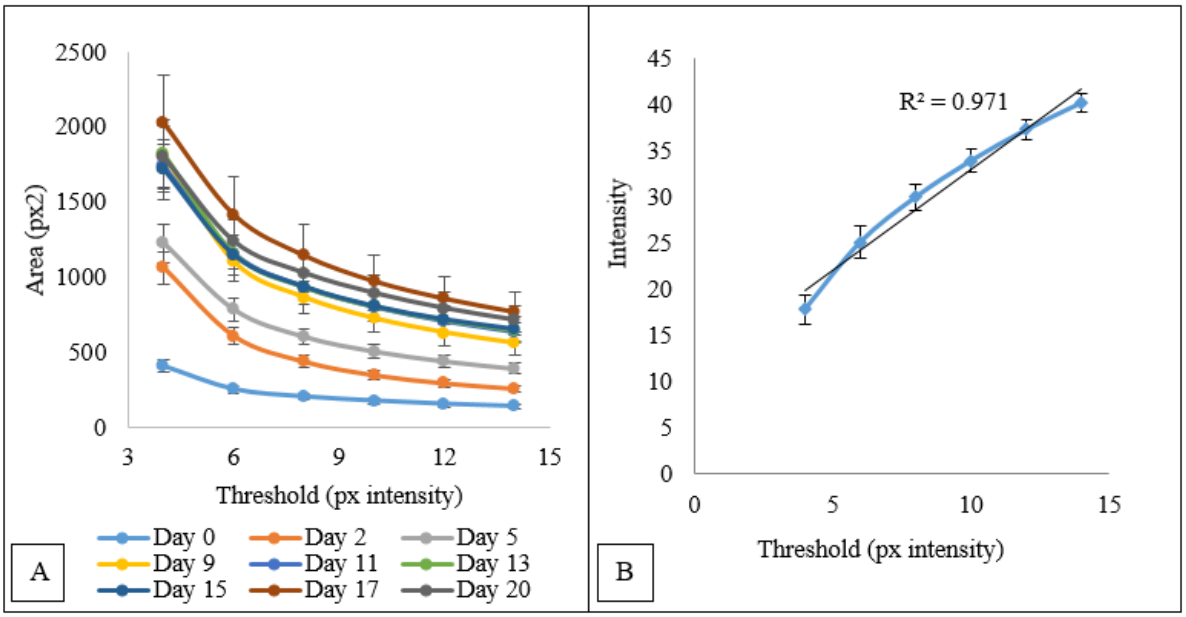

Figure 19: Nonlinear effect of intensity threshold on area, the obvious linear effect of intensity threshold on intensity

A graph of combined effects of minimum threshold on total fluorescence is presented in appendix Figure A.3. After determining the effects of these two parameters on image analysis, all images were taken with a minimum pixel intensity of 8 and a gain of 3. Given the apparent nonlinear relationship of intensity (gain and threshold) with pixel area, it was critical that all measurements were taken with the same parameters. An equation combining the results in Figure 19A and 19B could be devised, but that was not explored as it was not necessary for the body of this work.

The first study involved *C. sorokiniana* and *S. minutum* coded as "CE", the results of which appear in Figures 20 and 21, which displays cell density per droplet with respect to each culture. Error bars represent standard error as a means of indicating the central tendency of each point. An important caveat for either figure is that these monocultures were indistinguishable without increasing microscopic magnification such that, for analysis, the "CE" biculture was considered a uniform culture. Provided that the biculture feedstock will create droplets of both monocultures and bicultures due to heterogeneity, this handling would underestimate possible biculture productivity.

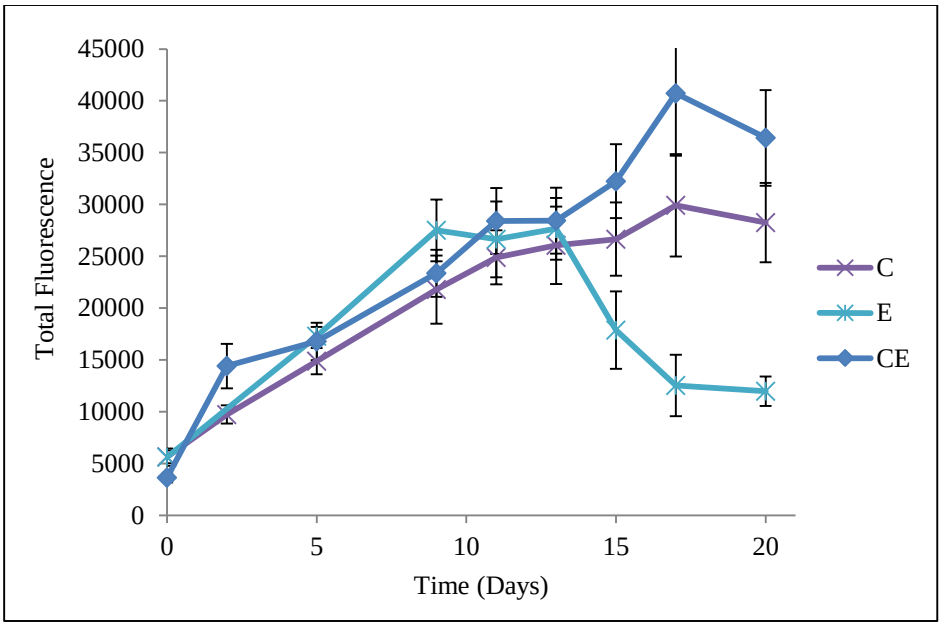

Figure 20: Total fluorescence for *C. sorokiniana* and *S. minutum* in microdroplets (n=20)

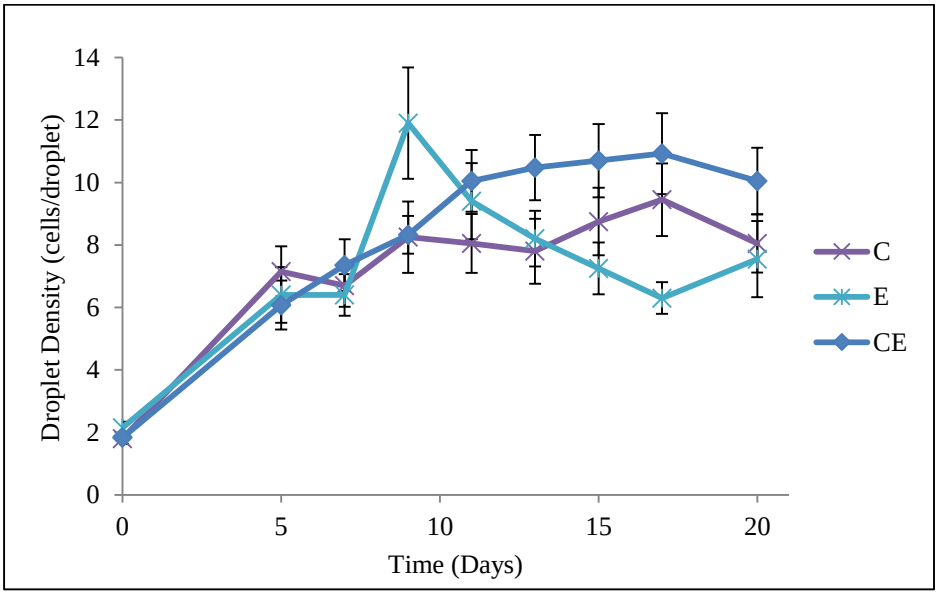

Figure 21: Cell densities for *C. sorokiniana* and *S. minutum* in microdroplets (n=20)

These graphs confirm the results from Figure 8 (see page 29), showing the biculture reaching a higher fluorescence and therefore carrying capacity by the end of the experiment even with the underestimation. This is further supported in Figure 21 by a higher overall cell count at Day 20. Standard error was selected in this figure because of the sheer variation between randomly selected droplets over the growth period. Some droplets, for example, would hold single or few cells by the end of the experiment while others could hold well over

fifty. Possible reasons for the apparent quiescence and lack of cell division within specific droplets could stem from cell age at inoculation or bulk inhibition by the storage device. Storing droplets in three dimensions rather than a monolayer means certain droplets are bound to receive more light simply due to droplet or cell shading. Either on the microscale or macroscale, growth inhibition is a major factor in propagating error within these experiments. Despite this error, growth curves from the flask experiment indicate similar growth trends and, surprisingly, similar relationships between final growth fluorescence, indicated in Figure 22.

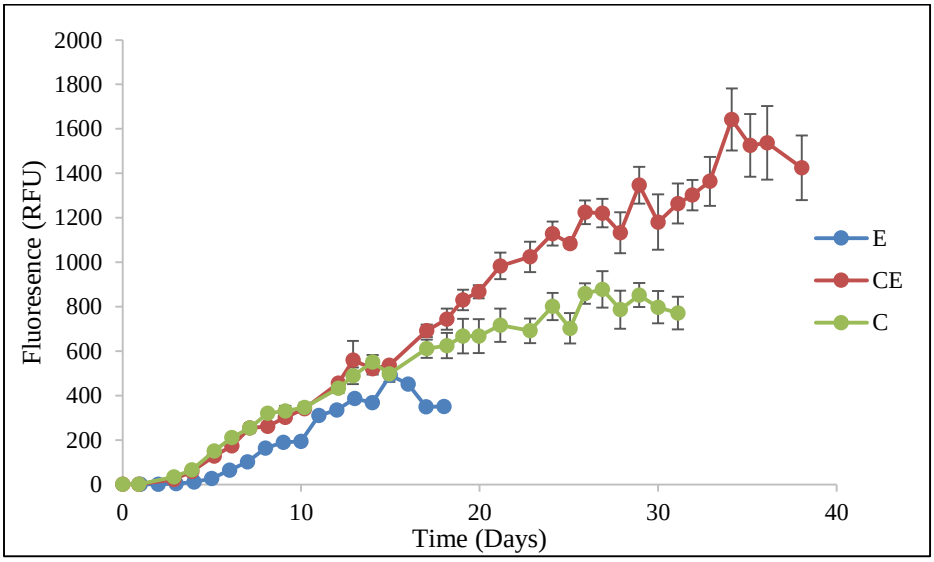

Figure 22: Growth curves of *C. sorokiniana* and *S. minutum* from flask experiment (n=4)

Next, the *A. falcatus* and *C. sorokiniana* combination was selected for analysis of transgressive overyielding. This combination proved unique due to ease of morphological identification such that trends noted in bulk comparisons between the biculture and the strict monocultures could also be used with respect to comparisons within the biculture. Such comparisons arise due to the nature of the Poisson distribution, which predicts that droplets within the biculture will either contain one of the constituent monocultures or the biculture. This factor allows for removal of the underestimation of biculture productivity, which would suggest even better performance due to isolation from monoculture constituents. Without clear morphological differences between species, this becomes increasingly difficult.

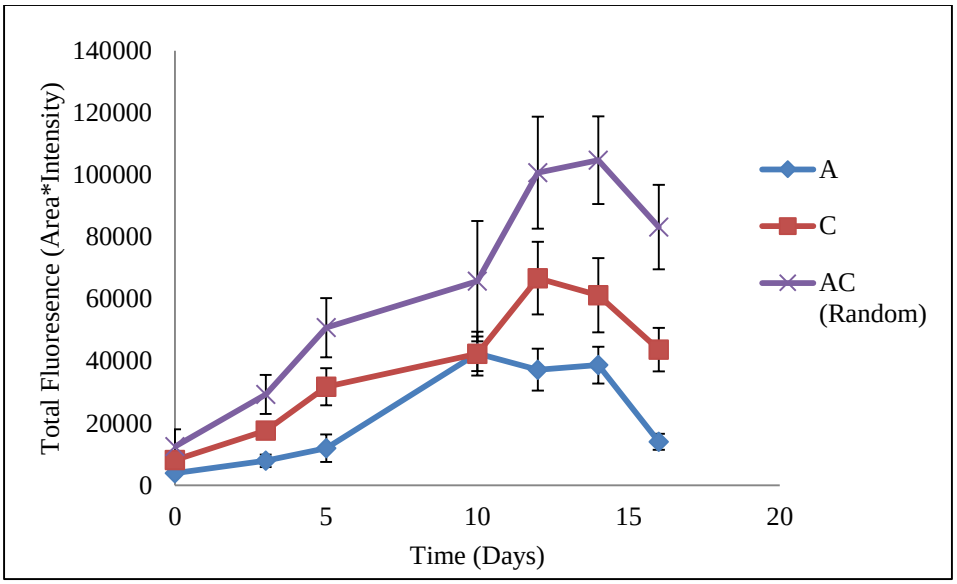

Figure 23: Comparison of monoculture droplets of *A. falcatus* and *C sorokiniana* with respect to randomized bulk biculture droplets

Again, these bulk droplets were selected independent of their composition and consisted of some random mixture of individual monocultures and the biculture. A mixture would thus expect to lower the overall total fluorescence of the sample with respect to the proposed overyielding biculture.

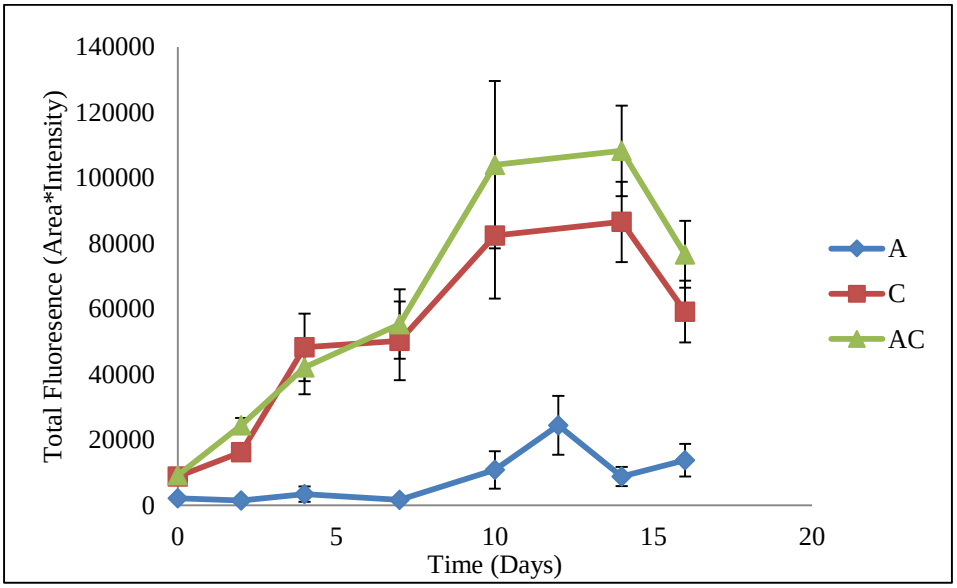

Figure 24: Comparison of *A. falcatus* and *C sorokiniana* monocultures and biculture droplets derived from the biculture feedstock

Figures 23 and 24 indicate that the exclusively biculture droplets outperform both the *C.*

sorokiniana droplets in biculture and the randomized bulk biculture droplets indicated in Figure 22. An important consideration is that between these figures, *A. falcatus* appears to perform significantly worse in the biculture feedstock whereas *C. sorokiniana* appears to perform significantly better. This observation has been repeatedly demonstrated in these experiments with likely two explanations. First, *A. falcatus* tends to flocculate leading to the selection of only the brightest droplets in monoculture, whereas these groups were less prevalent in the biculture images. Second, these trends could be the result of a characteristic unique to bulk bicultures like, for example, interdroplet effects of light shading. Unfortunately, these hypotheses require monolayer droplet storage for individual droplet tracking and, under bulk conditions, cannot be tested. A depiction of this experiment in flasks is available in appendix Figure A.4.

Lastly, *S. capricornutum* and *S. acuminatus* were generated in droplets for a final experiment to indicate whether droplets could also distinguish negative relationships.

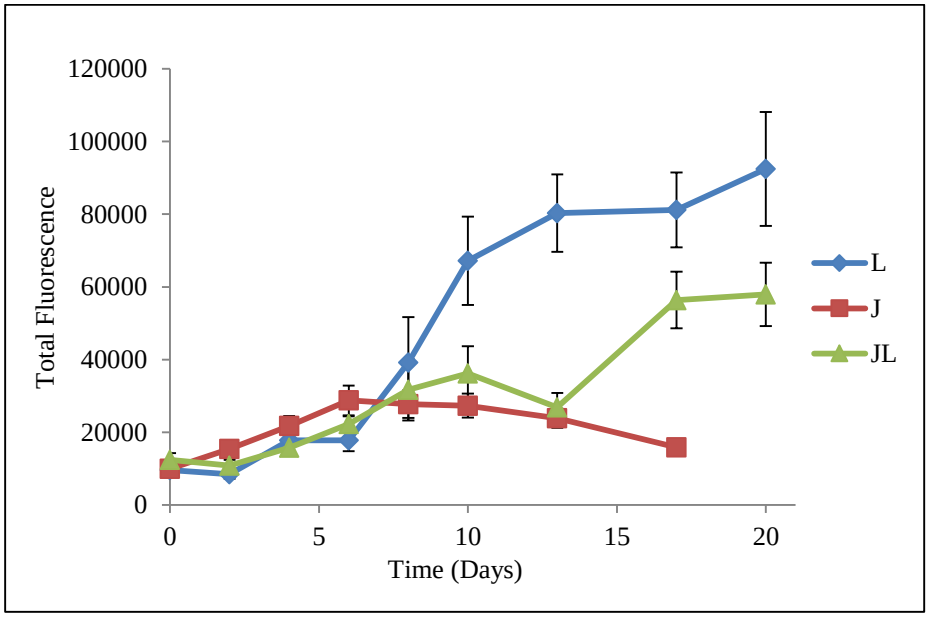

Figure 25: *S. ecornis* and *S. capricornutum* in droplets (n=20)

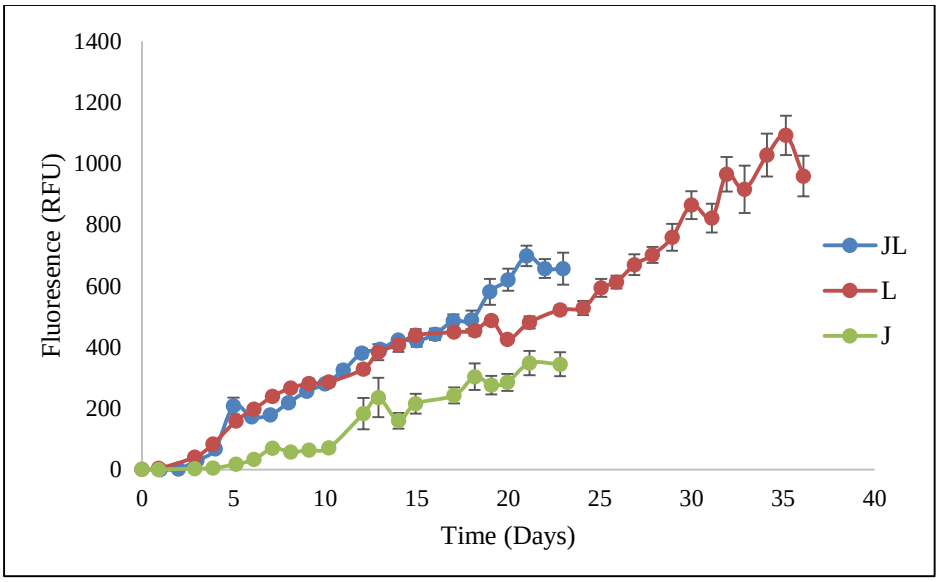

Figure 26: *S. ecornis* and *S. capricornutum* in flasks (n=4)

In this case, *S. capricornutum* clearly outperforms both the other monoculture and the combined biculture in droplets (Figure 25), as predicted from the flask experiment (Figure 26).

The three experiments described above validate the microfluidic platform in its ability to identify transgressive overyielding of algae co-cultures. For large scale experiments, they pose important questions for further optimization and droplet analytics.

4.6 Discussion

These experiments have successfully demonstrated the translation of bench sized overyielding experiments to microfluidic droplets. Implications of these results are that this platform could be effective in screening a massive quantity of algal combinations with several optimizations. The two major avenues for optimization pertain to droplet storage and droplet analysis. Creating a highly controlled, humidified environment in which droplets may be arranged and stored in a PDMS device would allow for predictable arrangement and droplet tracking. Construction of such a device will not only reduce error throughout the experiment, but allow for rapid and predictable screening of droplet fluorescence. Arranging droplets in this manner would allow for application of computational software like MATLAB in tandem with ImageJ for quick coding and analysis, thereby reducing manual selection and facilitating the high throughput nature of microfluidic work.

A second opportunity arises due to the unique intensity signatures of algal species within

our library. Each algal species appears to have a different fluorescence intensity suggesting that screening of many species combinations could allow for estimation of cell densities and population relationships rather than morphological differences, which can be difficult. These distinctive differences in relative species fluorescence could then be used with a fluorescence sorting device like fluorescence-activated cell sorting (FACS) or fluorescence spectroscopy with HPLC. FACS appears as readily the easiest application as droplets could be double emulsified such that the exterior fluid is aqueous. This would allow for drop-in droplet sorting in a FACS machine without necessary further adjustment as well as initial sorting on the basis of fluorescence signatures. A final sorting could facilitate the isolation of particularly productive communities, which could be individually screened and analyzed for elucidation of interspecies interactions.

References

1. "U.S. Product Supplied For Crude Oil And Petroleum Products". *Eia.gov*. N.p., 2016. Web. 10 Apr. 2016.

2. "U.S. Crude Oil, Natural Gas, And Natural Gas Liquids Proved Reserves". *Eia.gov*. N.p., 2016. Web. 10 Apr. 2016.

3. "Louisiana - State Energy Profile Analysis - U.S. Energy Information Administration (EIA)". *Eia.gov*. N.p., 2016. Web. 10 Apr. 2016.

4. "Intergovernmental Panel On Climate Change". *Climate Change 2014 Synthesis Report Summary for Policymakers*. N.p., 2016. Web. 10 Apr. 2016.

5. Solomon, Susan et al. "Irreversible Climate Change Due To Carbon Dioxide Emissions". *Proceedings of the National Academy of Sciences* 106.6 (2009): 1704-1709. Web. 10 Apr. 2016.

6. "Understanding The IPCC Reports | World Resources Institute". *Wri.org*. N.p., 2016. Web. 10 Apr. 2016.

7. "COP21 | One Hundred Billion Dollars". *Cop21.gouv.fr*. N.p., 2016. Web. 10 Apr. 2016.

8. "Rins And Rvos Are Used To Implement The Renewable Fuel Standard - Today In Energy - U.S. Energy Information Administration (EIA)". *Eia.gov*. N.p., 2013. Web. 10 Apr. 2016.

9. "Monthly Biodiesel Production Report". *U.S. Energy Information Administration*. N.p., 2016. Web. 10 Apr. 2016.

10. Capehart, Thomas. "USDA ERS - U.S. Bioenergy Statistics". *Ers.usda.gov*. N.p., 2016. Web. 10 Apr. 2016.

11. "Life Cycle Assessment — Principles And Framework". *International Organization for Standardization*. N.p., 2016. Web. 10 Apr. 2016.

12. Brennan, Liam, and Philip Owende. "Biofuels from microalgae—a review of technologies for production, processing, and extractions of biofuels and co-products." *Renewable and sustainable energy reviews* 14.2 (2010): 557-577.

13. Mata, Teresa M., António A. Martins, and Nidia. S. Caetano. "Microalgae For Biodiesel Production And Other Applications: A Review". *Renewable and Sustainable Energy Reviews* 14.1 (2010): 217-232. Web. 10 Apr. 2016.

14. Cuff, D.J., and W.J. Young. "United States Energy Atlas. [Review; Contains Glossary]". *Free Press,New York, NY* (1980): n. pag. Web. 10 Apr. 2016.

15. Grossman, A. R. et al. "Chlamydomonas Reinhardtii At The Crossroads Of Genomics". *Eukaryotic Cell* 2.6 (2003): 1137-1150. Web. 10 Apr. 2016.

16. Jones, Carla S, and Stephen P Mayfield. "Algae Biofuels: Versatility For The Future Of Bioenergy". *Current Opinion in Biotechnology* 23.3 (2012): 346-351. Web. 10 Apr. 2016.

17. Hlavova, Monika, Zoltan Turoczy, and Katerina Bisova. "Improving Microalgae For Biotechnology — From Genetics To Synthetic Biology". *Biotechnology Advances* 33.6 (2015): 1194-1203. Web. 10 Apr. 2016.

18. Beer, Laura L et al. "Engineering Algae For Biohydrogen And Biofuel Production". *Current Opinion in Biotechnology* 20.3 (2009): 264-271. Web. 10 Apr. 2016.

19. Niyogi, Krishna K. "PHOTOPROTECTION REVISITED: Genetic And Molecular Approaches". *Annual Review of Plant Physiology and Plant Molecular Biology* 50.1 (1999): 333-359. Web. 10 Apr. 2016.

20. Gimpel, Javier A et al. "Advances In Microalgae Engineering And Synthetic Biology Applications For Biofuel Production". *Current Opinion in Chemical Biology* 17.3 (2013): 489-495. Web. 10 Apr. 2016.

21. Ort, D. R., X. Zhu, and A. Melis. "Optimizing Antenna Size To Maximize Photosynthetic Efficiency". *PLANT PHYSIOLOGY* 155.1 (2010): 79-85. Web. 10 Apr. 2016.

22. Georgianna, D. Ryan, and Stephen P. Mayfield. "Exploiting Diversity And Synthetic Biology For The Production Of Algal Biofuels". *Nature* 488.7411 (2012): 329-335. Web. 10 Apr. 2016.

23. Hognon, Céline et al. "Comparison Of Pyrolysis And Hydrothermal Liquefaction Of Chlamydomonas Reinhardtii. Growth Studies On The Recovered Hydrothermal Aqueous Phase". *Biomass and Bioenergy* 73 (2015): 23-31. Web. 10 Apr. 2016.

24. Valdez, Peter J. et al. "Hydrothermal Liquefaction Of Bacteria And Yeast Monocultures". *Energy & Fuels* 28.1 (2014): 67-75. Web. 10 Apr. 2016.

25. Valdez, Peter J. et al. "Hydrothermal Liquefaction Of Nannochloropsis Sp.: Systematic Study Of Process Variables And Analysis Of The Product Fractions". *Biomass and Bioenergy* 46 (2012): 317-331. Web. 10 Apr. 2016.

26. Mittelbach, Gary George. *Community Ecology*. Sunderland, Mass.: Sinauer Associates, 2012. Print.

27. Tilman, David. "Biodiversity And Stability In Grasslands". *University of Minnesota*. N.p., 2016. Web. 10 Apr. 2016.

28. Tilman, D. "The Influence Of Functional Diversity And Composition On Ecosystem Processes". Science 277.5330 (1997): 1300-1302. Web. 10 Apr. 2016.

29. Tilman, D. "Diversity And Productivity In A Long-Term Grassland Experiment". *Science* 294.5543 (2001): 843-845. Web. 10 Apr.2016.

30. Naeem, Shahid et al. "Declining Biodiversity Can Alter The Performance Of Ecosystems". *Nature* 368.6473 (1994): 734-737. Web. 10 Apr. 2016.

31. McCann, Kevin Shear. "The Diversity–Stability Debate". *Nature* 405.6783 (2000): 228-233. Web. 10 Apr. 2016.

32. Hardin, G. "The Competitive Exclusion Principle". *Science* 131.3409 (1960): 1292-1297. Web. 10 Apr. 2016.

33. Loreau, Michel, and Andy Hector. *Nature* 412.6842 (2001): 72-76. Web. 10 Apr. 2016.

34. Croft, Martin T. et al. "Algae Acquire Vitamin B12 Through A Symbiotic Relationship With Bacteria". *Nature* 438.7064 (2005): 90-93. Web. 10 Apr. 2016.

35. Cardinale, Bradley J. "Biodiversity Improves Water Quality Through Niche Partitioning". *Nature* 472.7341 (2011): 86-89. Web. 10 Apr. 2016.

36. Cardinale, B. J. et al. "Impacts Of Plant Diversity On Biomass Production Increase Through Time Because Of Species Complementarity". *Proceedings of the National Academy of Sciences* 104.46 (2007): 18123-18128. Web. 10 Apr. 2016.

37. Cardinale, B. J. et al. "The Functional Role Of Producer Diversity In Ecosystems". *American Journal of Botany* 98.3 (2011): 572-592. Web. 10 Apr. 2016.

38. Narwani, Anita et al. "Experimental Evidence That Evolutionary Relatedness Does Not Affect The Ecological Mechanisms Of Coexistence In Freshwater Green Algae". *Ecology Letters* 16.11 (2013): 1373-1381. Web. 10 Apr. 2016.

39. Chisti, Yusuf, and Jinyue Yan. "Energy From Algae: Current Status And Future Trends". *Applied Energy* 88.10 (2011): 3277-3279. Web. 10 Apr. 2016.

40. Chisti, Yusuf. "Biodiesel From Microalgae". *Biotechnology Advances* 25.3 (2007): 294-306. Web. 10 Apr. 2016.

41. Conchouso, David, et al. "Simulation of a 3D Flow-Focusing Capillary-Based Droplet Generator."

42. Whitesides, George M. "The origins and the future of microfluidics." *Nature* 442.7101 (2006): 368-373.

43. Huebner, Ansgar, et al. "Microdroplets: a sea of applications?." *Lab on a Chip*8.8 (2008): 1244-1254.

44. Teh, Shia-Yen, et al. "Droplet microfluidics." *Lab on a Chip* 8.2 (2008): 198-220.

45. "Microfluidics and microfluidic devices: a review." *elveflow*. N.p., n.d. Web. 15 Dec. 2014. <http://www.elveflow.com/microfluidic-reviews-and-tutorials/microfluidics-and-microfluidic-devices-a-review>.

46. Garstecki, Piotr, et al. "Formation of droplets and bubbles in a microfluidic T-junction—scaling and mechanism of break-up." *Lab on a Chip* 6.3 (2006): 437-446.

47. Thorsen, Todd, et al. "Dynamic pattern formation in a vesicle-generating microfluidic device." *Physical review letters* 86.18 (2001): 4163.

48. Gupta, Amit, SM Sohel Murshed, and Ranganathan Kumar. "Droplet formation and stability of flows in a microfluidic T-junction." *Applied physics letters* 94.16 (2009): 164107.

49. Nisisako, Takasi, and Toru Torii. "Microfluidic large-scale integration on a chip for mass production of monodisperse droplets and particles." *Lab on a Chip* 8.2 (2008): 287-293.

50. Seemann, Ralf, et al. "Droplet based microfluidics." *Reports on progress in physics* 75.1 (2012): 016601.

51. Conchouso, David, et al. "Simulation of a 3D Flow-Focusing Capillary-Based Droplet Generator."

52. Lee, Junghoon, et al. "Electrowetting and electrowetting-on-dielectric for microscale liquid handling." *Sensors and Actuators A: Physical* 95.2 (2002): 259-268.

53. Chung, Sang Kug, Kyehan Rhee, and Sung Kwon Cho. "Bubble actuation by electrowetting-on-dielectric (EWOD) and its applications: A review."*International Journal of Precision Engineering and Manufacturing* 11.6 (2010): 991-1006.

54. Shah, Gaurav J. "EWOD: Theory and fabrication." University of California, Los Angeles. Speech.

55. Walker, Shawn W., and Benjamin Shapiro. "Modeling the fluid dynamics of electrowetting on dielectric (EWOD)." *Microelectromechanical Systems, Journal of* 15.4 (2006): 986-1000.

56. Yue, Pengtao, et al. "A diffuse-interface method for simulating two-phase flows of complex fluids." *Journal of Fluid Mechanics* 515 (2004): 293-317.

57. Sun, Ying, and Christoph Beckermann. "Sharp interface tracking using the phase-field equation." *Journal of Computational Physics* 220.2 (2007): 626-653.

58. Abrishamkar, A., et al. "A COMSOL Multiphysics® Model of Droplet Formation at a Flow Focusing Device."

59. Glasner, Karl. "A diffuse interface approach to Hele–Shaw flow." *Nonlinearity*16.1 (2003): 49.

60. Li, Yuehao, et al. "Geometric optimization of liquid–liquid slug flow in a flow-focusing millifluidic device for synthesis of nanomaterials." *Chemical Engineering Journal* 217 (2013): 447-459.

61. Li, Y., et al. "Numerical Study of the Controlled Droplet Breakup by Electric Fields inside a Microfluidic Flow-focusing Device."

62. Sciancalepore, Anna Giovanna, et al. "Microdroplet-based multiplex PCR on chip to detect foodborne bacteria producing biogenic amines." *Food microbiology* 35.1 (2013): 10-14.

63. Lee, Won Gu, et al. "Nano/Microfluidics for diagnosis of infectious diseases in developing countries." *Advanced drug delivery reviews* 62.4 (2010): 449-457.

64. Jeong, Su Jin, et al. "Prospective Comparison of Qualitative Versus Quantitative Polymerase Chain Reaction for Monitoring Virologic Treatment Failure in HIV-Infected Patients." *AIDS research and human retroviruses*(2014).

65. Huebner, A., et al. "Quantitative detection of protein expression in single cells using droplet microfluidics." *Chemical communications* 12 (2007): 1218-1220.

66. Park, Jihyang, et al. "Microdroplet-enabled highly parallel co-cultivation of microbial communities." *PLoS One* 6.2 (2011): e17019.

67. Wheeler, Aaron R. "Putting electrowetting to work." *Science* 322.5901 (2008): 539-540.

68. Dittrich, Petra S., and Andreas Manz. "Lab-on-a-chip: microfluidics in drug discovery." *Nature Reviews Drug Discovery* 5.3 (2006): 210-218.

69. Algae, UTEX. "Algal Culture Media Recipes". *UTEX Culture Collection of Algae*. N.p., 2016. Web. 10 Apr. 2016.

70. "Modified Bold 3N Medium Recipe". *University of Texas*. N.p., 2016. Web. 10 Apr. 2016.

71. "F17T8/TL830/PLUS/ALTO 30PK T8 Plus - Philips Lighting". *Usa.lighting.philips.com*. N.p., 2016. Web. 10 Apr. 2016.

72. "Pediastrum Duplex Meyen :: Algaebase". *Algaebase.org*. N.p., 2016. Web. 10 Apr. 2016.

73. Duffy, David C. et al. "Rapid Prototyping Of Microfluidic Systems In Poly(Dimethylsiloxane)". *Analytical Chemistry* 70.23 (1998): 4974-4984. Web. 10 Apr. 2016.

74. "SU-8 2000 Permanent Epoxy Negative Photoresist". *Micro Chem*. N.p., 2016. Web. 10 Apr. 2016.

75. Srinivasan, U. et al. "Alkyltrichlorosilane-Based Self-Assembled Monolayer Films For Stiction Reduction In Silicon Micromachines". *Journal of Microelectromechanical Systems* 7.2 (1998): 252-260. Web. 10 Apr. 2016.

76. Lagus, Todd P., and Jon F. Edd. "High-Throughput Co-Encapsulation Of Self-Ordered Cell Trains: Cell Pair Interactions In Microdroplets". *RSC Advances* 3.43 (2013): 20512. Web. 10 Apr. 2016.

77. Pan, Jie et al. "Quantitative Tracking Of The Growth Of Individual Algal Cells In Microdroplet Compartments". *Integr. Biol.* 3.10 (2011): 1043. Web. 10 Apr. 2016.

78. Sung, Young Joon et al. "Microdroplet Photobioreactor For The Photoautotrophic Culture Of Microalgal Cells". *The Analyst* 141.3 (2016): 989-998. Web. 10 Apr. 2016.

Appendix:

Table A.1: Full list of strains from algal library

Strain Name	**Letter Code**
Ankistrodesmus falcatus	A
Botryococcus sudeticus	B
Chlorella sorokiniana	C
Coelastrum microporum	D
Selenastrum minutum	E
Oocystis polymorpha	F
Pediastrum duplex	G
Pediastrum tetras	H
Scenedesmus acuminatus	I
Scenedesmus ecornis	J
Scenedesmus obliquus	K
Selenastrum capricornutum.	L

Culture	N0	K	K (95% CI)	r	r (95% CI)	SSE (*10^5)	R square	Adj R Square	RMSE
A	1.08	485.7	(464.3, 507)	0.468	(0.4471, 0.4882)	4.042	0.881	0.880	66.3
AC	1.17	1286	(379.2, 423.1)	0.441	(0.4214, 0.4607)	24.201	0.879	0.878	175.0
AE	0.78	483.2	(461.6, 504.8)	0.530	(0.5083, 0.5515)	3.332	0.906	0.905	60.8
AG	3.69	903.5	(842, 965)	0.215	(0.2066, 0.2243)	27.199	0.799	0.798	134.7
AI	0.91	1008	(968, 1048)	0.434	(0.4194, 0.4489)	17.385	0.912	0.911	123.5
AL	1.32	1011	(939.6, 1082)	0.329	(0.311, 0.3466)	61.491	0.688	0.686	214.2
C	0.80	706.7	(672.2, 741.2)	0.660	(0.6173, 0.7027)	20.242	0.782	0.780	135.7
CE	0.70	1264	(1206, 1323)	0.453	(0.4327, 0.4736)	67.244	0.815	0.814	224.0
CG	3.71	1287	(1216, 1358)	0.370	(0.3512, 0.3887)	49.979	0.841	0.840	209.4
CI	0.87	1426	(1342, 1510)	0.450	(0.4282, 0.4716)	76.392	0.811	0.810	258.9
CL	1.25	1177	(1104, 1250)	0.475	(0.447, 0.5031)	62.594	0.769	0.767	238.5
E	0.68	397.1	(375.4, 418.8)	0.669	(0.6362, 0.7025)	1.957	0.906	0.905	52.9
EG	4.88	751.1	(686.2, 816)	0.307	(0.2872, 0.3274)	18.117	0.800	0.798	133.3
EI	0.78	1040	(990.8, 1089)	0.438	(0.4189, 0.4573)	20.857	0.888	0.887	149.0
EL	1.00	1022	(926.3, 1118)	0.334	(0.3129, 0.3559)	48.684	0.667	0.664	225.2
G	8.59	1357	(1228, 1486)	0.176	(0.1683, 0.1838)	50.084	0.821	0.820	182.7
GI	4.65	1054	(1016, 1091)	0.328	(0.3156, 0.3396)	20.218	0.913	0.913	124.7
GL	3.82	1276	(1183, 1368)	0.210	(0.2022, 0.2173)	43.250	0.848	0.847	169.8
I	1.07	850.8	(816.9, 884.8)	0.470	(0.4536, 0.487)	10.291	0.921	0.920	100.4
IL	1.39	629.6	(600.3, 658.9)	0.514	(0.4913, 0.5369)	6.169	0.889	0.887	82.8
J	1.87	318.4	(288.5, 348.3)	0.415	(0.3848, 0.445)	2.521	0.821	0.818	56.8
JL	0.43	530.9	(499.6, 562.1)	0.714	(0.6652, 0.7625)	10.908	0.757	0.755	107.7
L	1.04	760.6	(708.5, 812.7)	0.405	(0.3775, 0.4331)	46.256	0.620	0.617	188.6

Figure A.1: Species cultures with calculated carrying capacities (K) and growth rates (r) with 95% confidence parameters and logistic regression statistics

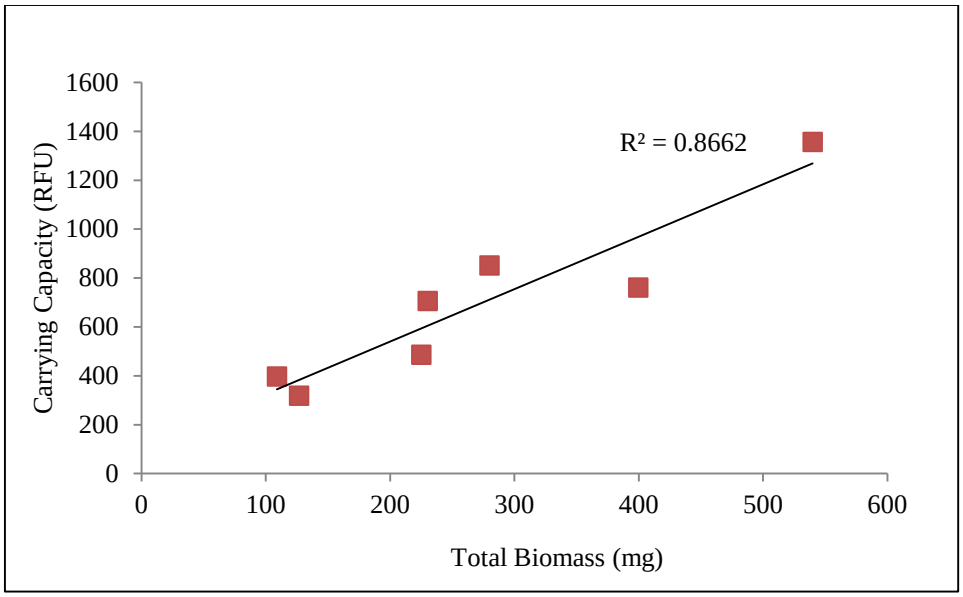

Figure A.2: Comparison of carrying capacities and total biomass of monocultures

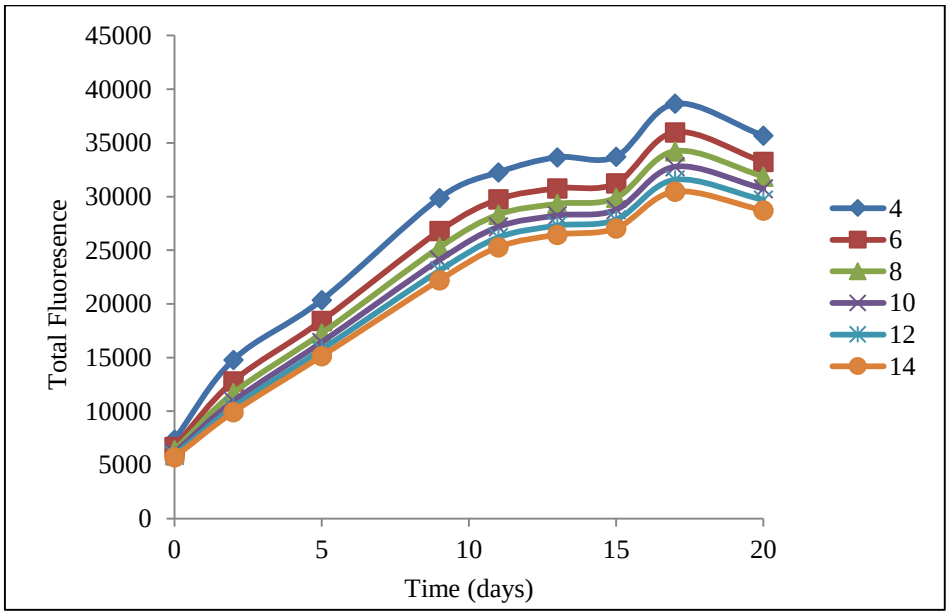

Figure A.3: Changes in total fluorescence for each threshold

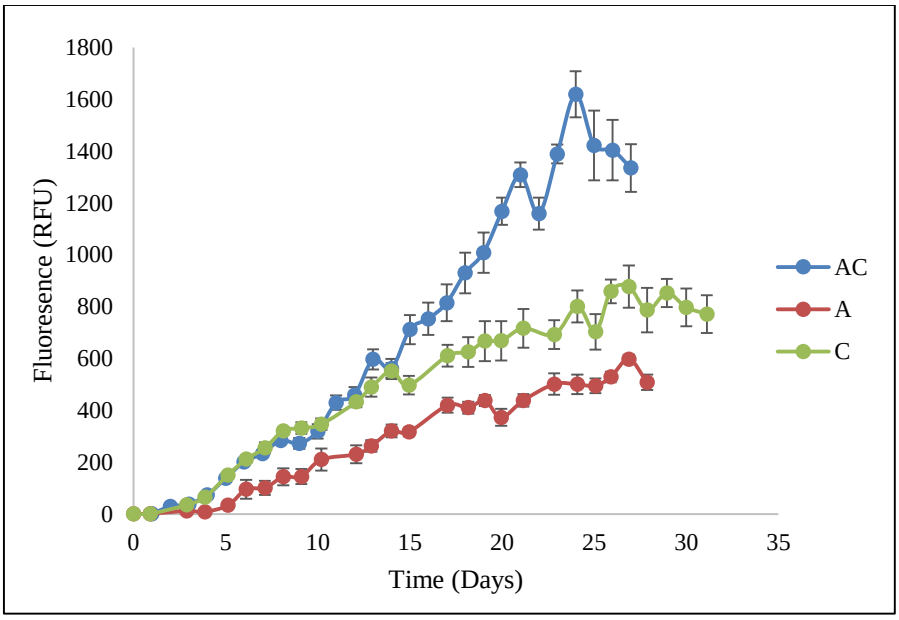

Figure A.4: *A. falcatus* and *C. sorokiniana* from the flask experiment (n=4)